Surv Geophys (2012) 33:65–105
DOI 10.1007/s10712-011-9144-0

Magnetotelluric Studies at the San Andreas Fault Zone: Implications for the Role of Fluids

Michael Becken · Oliver Ritter

Received: 17 January 2011 / Accepted: 29 August 2011 / Published online: 1 December 2011

Abstract Fluids residing in interconnected porosity networks have a significant weakening effect on the rheology of rocks and can strongly influence deformation along fault zones. The magnetotelluric (MT) technique is sensitive to interconnected fluid networks and can image these zones on crustal and upper mantle scales. MT images have revealed several prominent electrical conductivity anomalies at the San Andreas Fault which have been attributed to the presence of saline fluids within such networks and which have been associated with tectonic processes. These models suggest that ongoing fluid release in the upper mantle and lower crust is closely related to the mechanical state of the crust. Where fluids are drained into the brittle crust, and where these fluids are kept at high pressures, fault creep is supported. Fluid fluxes from deeper levels, in combination with meteoric and crustal metamorphic fluid inflow, and in response to fault creep, leads to high-conductivity zones developing as fault zone conductors in the brittle portion of crust. In turn, the absence of crustal fluid pathways may be characteristic for mechanically locked segments of the fault. Here, MT models suggest that fluids are trapped at depth and kept at high pressures. We speculate that fluids may infiltrate neighboring rocks and in their wake induce non-volcanic tremor.

Keywords Magnetotellurics · San Andreas Fault · Fluids

1 Introduction

California is one of the most earthquake-prone regions of the world. Most occurrences of earthquakes are attributed to the San Andreas Fault (SAF) system, which runs the entire length of California. Major earth science initiatives such as the San Andreas Fault

M. Becken · O. Ritter
GFZ German Research Centre for Geosciences, Telegrafenberg, 14473 Potsdam, Germany

Present Address:
M. Becken (✉)
Institute of Geophysics, WWU, Corrensstr. 24, 48149 Münster, Germany
e-mail: michael.becken@uni-muenster.de

Observatory at Depth (SAFOD), a deep borehole intersecting the SAF at 3.2 km depth (Hickman et al. 2004), and a range of geological, geochemical, and geophysical exploration and monitoring programs have tremendously increased our knowledge about physical and chemical processes within and surrounding the fault zone, making the SAF the best studied fault zone on Earth. However, fundamental properties of the fault such as fault strength and fault geometry at deeper levels are not fully understood.

Many of the seismological observations, including aseismic slip along distinct segments of the SAF (Irwin and Barnes 1975) and companion faults and the occurrence of 'non-volcanic' tremor (NVT) at lower crustal and upper mantle depth (Nadeau and Dolenc 2005) are explained with fluid-related processes, as fluids can strongly influence the mechanical strength of rocks. Fluids at high pressures have the ability to reduce the strain threshold of rocks and facilitate brittle failure within the upper crust (Byerlee 1990; Scholz 2002). At deeper levels, below the seismogenic zone where rocks exhibit a ductile (or viscous) style of deformation, the presence of fluids can also dramatically reduce the shear strength. The effect of weakening will be more severe if fluids form an interconnected network, i.e., in pores, cracks, or veins (Bürgmann and Dresen 2008). In turn, a high degree of pore interconnectivity may indicate a region with a high degree of strain, i.e., a zone that has undergone substantial deformation during its tectonic history.

Bulk electrical conductivity of a subsurface volume depends strongly on the presence of conductive phases within such interconnected networks (Gueguen and Palciauskas 1994), and measurements of electrical conductivity are therefore one of the best means to constrain the volume of available fluids and the regions of high strain. In turn, electrical conductivity can be used to constrain rock strength in the lower crust and upper mantle. In addition to aqueous fluids and partial melts, conductive minerals may be responsible for conductive MT anomalies. Exhumed fossil shear zones, for instance, are often highly mineralized (Weckmann et al. 2003). A region in the crust weakened by shearing and faulting can be intruded by carbon-bearing or hydrothermal fluids which in turn generate mineralized veins and fissures by chemical precipitation reactions (e.g., Ritter et al. 2005) and result in chemical weakening (Scholz 2002) and enhanced electrical conductivity. Shearing also provides the energy that drives chemical reactions between the surface and the lubricant molecules inside a sliding contact and can, for example, be responsible for the deposition of graphite films in shear zones (e.g., Ritter et al. 1999). Continued shearing deformation can further increase the interconnectivity of such mineralized zones. However, recent laboratory experiments showed that thin graphite films are unstable at high temperatures (>730°C) and are therefore not likely to account for observations of low resistivity anomalies at lower crustal levels (Yoshino and Noritake 2011).

Jiracek et al. (2007) and Unsworth (2010) summarized relationships between lower crustal fluids and bulk electrical conductivity, and the effect of fluids on rock strength. Here, we only briefly summarize the principles and refer otherwise to these papers and references therein. If fluids are responsible for high electrical conductivity of a subsurface volume, then the implication for rock strength and fault properties can be multifold. First, the presence of fluids (at high pressures) has a weakening effect itself, because that counteracts the fault-normal stress and thereby reduces the effective shear strength of a fault plane (e.g., Byerlee 1990). Mechanical weakening due to high pressure fluids is not solely effective on discrete fault planes, but can also affect an entire rock volume. Second, the mechanical weakening effects of high-pressure fluids become stronger, if fluids form an interconnected network (Bürgmann and Dresen 2008). Jiracek et al. (2007) pointed out that, for lower crustal conditions, both a fluid-filled fracture network and grain-edge interconnection, or a combination of both, can result in interconnected fluids. It is

important to note that fracture networks can form in ductile regimes at low strain rates provided the fluid pressure is elevated compared with the vertical stress. Interconnection on grain-boundary scale is controlled by the dihedral angle or wetting angle. Wetting is the ability of fluids to form boundary surfaces with solid states; it is determined by measuring the contact angle, which the liquids form when in contact with the solids. Wetting angles below 60 degrees allow for the formation of connected fluid tubes between grain edges; at higher angles, the fluid phase is isolated at grain edges without interconnection (see Jiracek et al. 2007 for more details). The wetting angle is dependent on the fluid composition and the mineralogy of rocks as well as on pressure and stress conditions. Typically, the addition of salt to the fluid decreases the wetting angle, suggesting that saline fluids in the ductile regime are more likely to be interconnected. In turn, high pressures result in reduced wetting of grain boundaries, whereas shear stress can result in increased wetting ability.

The weakening effects of fluids suggest that deep conductive zones imaged with MT often correspond to mechanically weak zones. Türkoglu et al. (2008) pointed out that it is important to separate cause and effect when addressing the relationship between aqueous fluids and/or partial melts and deformation. Fluids can actively contribute to rock weakening through the formation of interconnected networks, hydro-fracturing, chemical weakening, and pressure buildup associated with mechanical weakening. Alternatively, fluids can illuminate (in the sense of elevated electrical conductivity) strain-generated porosity, which may represent per se weak zones. In summary, low resistivities in the lower crust and upper mantle can reflect zones of aqueous fluids, partial melts and/or mineralizations due to fluid-driven chemical precipitation reactions. MT is not able to distinguish unambiguously between conductive fluids and other conductive phases at depth. Irrespective of the conductive phase, however, the high conductivity must possess long-range interconnection to be visible to MT measurements.

Magnetotelluric studies at the SAF, and at many other active and fossil tectonic systems, imaged electrical conductivity anomalies on various crustal and upper mantle scales, which seem closely related to active or ancient tectonic processes. Many of the high-conductivity anomalies associated with active tectonic settings are interpreted with saline or hydrothermal aqueous fluids residing in interconnected porosity networks. A deeper understanding of the resistivity structure can be obtained by addressing (1) the fluid sources, and the mechanisms or chemical reaction releasing these fluids, (2) mechanisms which can account for the required degree of pore interconnectivity, (3) the distribution and generation of pathways and barriers for fluid flow.

All of these aspects have fault-related implications. For instance, where the SAF exhibits aseismic creep or a combination of microseismicity and creep, the upper few kilometers of the fault are characterized by a wedge-shape zone of high conductivity associated with fluids circulating in the damage zone of the fault; this zone of high conductivity is often denoted as the fault zone conductor (FZC) (e.g., Ritter et al. 2005; Bedrosian et al. 2004; Unsworth et al. 2000). The FZC is characteristically devoid of seismicity, suggesting that this region is rheologically extremely weak (Unsworth et al. 2000). Along-strike variations of the FZCs, particularly variations of the conductances, have been associated with fault activity (Hoffmann-Rothe et al. 2004; Ritter et al. 2005), as active strain provides a means to develop and maintain permeability structure, and thus electrical conductivity, within the damage zone. Consequently, these conductivity models played an important role in pin-pointing the SAFOD drilling location near Parkfield.

In this paper, we consider MT studies at the SAF near Hollister and Carrizo Plain, respectively, and from the Parkfield-Cholame segment in central California. The existing MT studies at Carrizo Plain (Mackie et al. 1997; Unsworth et al. 1999) and Hollister

(Bedrosian et al. 2004) focused on imaging the upper crustal resistivity structure and its relationship with the SAF and companion fault zones. By far the most MT data are available from the Parkfield–Cholame segment in central California, where a number of fine-scale (Unsworth et al. 1997, 1999, 2000; Unsworth and Bedrosian 2004a) and regional scale studies (Eberhart-Philips et al. 1995; Becken et al. 2008, 2011) were carried out to investigate the zone of seismogenesis along the SAF as well as the deeper roots of the fault system in the lower crust and upper mantle.

A recent offshore marine MT survey (Wheelock et al. 2010) complements the regional scale land studies in central California. While these data are not yet available for this review, amphibian MT data are of particular interest to address (1) actively deforming offshore strands of the SAF system (e.g. Hosgri fault, see Wilson et al. 2005), (2) the role of the Monterey Microplate, thought to be partially subducted beneath continental North America, thereby influencing the development of the transform margin (e.g., McCrory et al. 2009; Popov 2009), (3) the coast effect, a term used to describe the effect of the high-conductance ocean sea water on the MT responses measured on land (e.g., Schmucker 1970).

The SAF has also been a target for telluric (Madden et al. 1993; Park et al. 2007) and magnetotelluric (MT) monitoring (e.g., Kappler et al. 2010) experiments. These installations attempted to resolve long-term electric (and magnetic) field variations of internal origin due to resistivity variations associated with earthquakes, large-scale fluid relocation, or other causes. To date, however, significant field variations which can be uniquely attributed to tectonic processes could not be detected.

The main objective of this paper is to review MT results from the SAF in combination with other geophysical, geological, and geochemical data and models in order to address active tectonic processes and the mechanical state of the fault and their implications for the geodynamic setting of the SAF system. Several observations suggest that fluids derived from the mantle strongly influence the mechanics of the fault system. This hypothesis is largely based on studies of the Parkfield–Cholame segment, where the SAF is transitional from a mechanically locked state to aseismic creep, and where a remarkable consistency exists between fluid distribution (high-conductivity zones), fluid chemistry, seismological patterns, geodynamical and mechanical modeling.

The paper is organized in three main parts. In Sect. 2, we discuss the relationship between resistivity structure, fluids and possible implications for the strength of the brittle SAF. In the second part (Sect. 3), regional-scale fluid-related processes are discussed based on MT models and other studies from the Parkfield–Cholame area. Thirdly (Sect. 4), we briefly review MT studies at the Niigata-Kobe tectonic zone (NKTZ) in Japan and the North Anatolian fault zone in Turkey as comparative cases.

2 Fluid Distribution and Fault Strength

Earthquakes along the SAF mostly range between depths of 2 and 15 km and provide information about the location and style of deformation of the fault in this upper crustal 'seismogenic' zone, where rocks fail in a brittle way. The seismogenic zone of the SAF is well defined by earthquake 'curtains' along the segments of the fault which exhibit a combination of aseismic slip and frequent microseismicity.

The aseismically creeping zones of the SAF and companion faults have not experienced any major earthquakes in historical times, and probabilities for major ruptures are low (Field et al. 2008). Those zones that have ruptured in major earthquakes in historical times

are in a mechanically locked state since then. The largest recorded earthquakes along the SAF occurred in 1857 in southern California and 1906 in San Francisco with magnitudes of approximately 8. The 1857 Fort Tejon earthquake nucleated near Parkfield and propagated southeastward over a length of 360 km. The great 1906 San Francisco earthquake ruptured the northern segment of the fault, from Hollister northward, for approximately 400 km. Since then, both segments appear to be locked (except for smaller ruptures associated with earthquakes such as the M7.1 Loma Prieta earthquake in 1989 and the M6.6 earthquake near Los Angelos in 1994). Between Parkfield and north of Hollister, the SAF exhibits a combination of aseismic creep and microseismicity. At Parkfield, characteristic M6 earthquakes have been observed repeatedly, the last one in 2004, whereas more continuous movement of about 2–4 cm per year and minor quakes characterize the rest of the creeping segment (Irwin 1990, cf. Fig. 1).

Early explanations of the difference in seismic behavior of the SAF emphasized the role of fluids released by metamorphic reactions (Fig. 5c, after Irwin and Barnes 1975). Fluids at high pressures also play a key role in more recent modeling scenarios which attempt to address the weakness of the fault where it exhibits aseismic creep (e.g., Fulton and Saffer 2009). MT is perhaps the only means to image fluids directly in the subsurface, and a number of MT studies across the SAF studies have delineated high-conductivity zones associated with the upper few kilometers of the SAF. Before discussing the implications of these MT results in more detail, however, we give a brief geological summary.

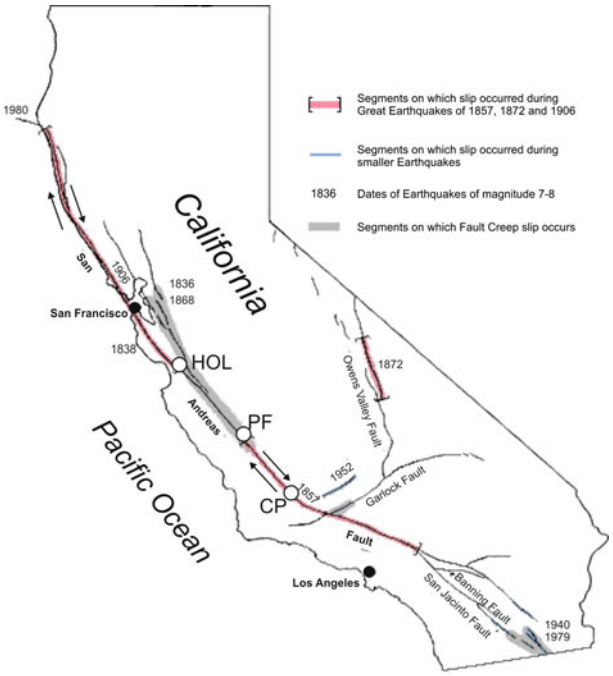

Fig. 1 Map of California showing segments of the SAF system where the fault exhibits creep (*gray shaded*) and distribution of ruptures associated with historical earthquakes (*red shaded*). Locations of MT study areas near Hollister (*HOL*), Parkfield (*PF*), and Carrizo Plain (*CP*) are indicated. Background map provided by US Geological Survey (http://pubs.usgs.gov/gip/earthq3/where.html)

2.1 Geological Setting

In central California, total displacement of the Pacific plate relative to fixed North America is estimated to about 820 ± 50 km (Nicholson et al. 1994). The displacement was distributed over various fault strands (Dickinson et al. 2005) since subduction of the Farallon oceanic plate ceased and the SAF system was initiated 20 Ma ago. Among these strands of the fault system, the central SAF has accommodated about 315 km displacement. Since the transform margin evolved, the geological formations along the continental margin were substantially reorganized, and the deformation along the SAF system has shaped the landscape of today's California.

Today, the SAF system criss-crosses three major geologic formations which constitute the Californian Coast Ranges: the Franciscan complex, the Salinian Block and the Great Valley sequence. These geological units form northwest–southeast trending belts (see geological map in Fig. 2a). The Franciscan rocks represent pieces of oceanic lithosphere that have been accreted to North America by subduction and collision prior to the development of the transform margin. They comprise sandstones and shale, carrying fragments of cherts and other rocks, low-grade metamorphosed volcanic rocks in greenschist facies, higher-grade blueschists, as well as disrupted pieces of the Coast Range ophiolite representing oceanic crust and mantle rocks. The major components of the Salinian Block are granitic plutonic rocks, similar in composition, chemistry and age to those of the Sierran batholith of the Sierra Nevada. As part of the Pacific plate, the Salinian block has been transported along the SAF in the northeast direction to its present position. Sediments of the Great valley sequence were originally deposited in the forearc basin of the Farallon subduction zone under marine conditions. All of these rocks have experienced substantial deformation and displacement during their subduction and transform motion history.

The SAF in central California juxtaposes the Salinian block, which is part of the Pacific plate, against Franciscan formations accreted to the North American plate. The Salinian Block is intervening between the SAF and westward located strands of the transform fault system. Figure 2b presents a simplified geological cross-section across the SAF near Cholame in central California, which is based on seismic reflection and refraction data, magnetic, gravity, and geological mapping (Page et al. 1998; Zoback et al. 2002). Whereas upper crustal structure is relatively well constrained by seismic data and geological observations, deeper structures, in particular evidence for remnants of the former subducting slab, are more difficult to decipher.

2.2 Earthquakes and Fault Creep

The apparent low frictional strength of the creeping SAF is poorly understood. The lack of an observable heat flow anomaly near the fault, as would be expected from frictional heat generation, suggests an effective friction coefficient along the SAF of 0.2 (e.g., Sass et al. 1997) or less. Mechanical modeling studies of the fault resulted in friction coefficients of less than 0.1 within the fault (Fulton and Saffer 2009; Popov 2009) in order to explain an active fault plane oriented at a high angle to the maximum principal stress direction (e.g., Fulton and Saffer 2009) as observed for the SAFOD (Hickman et al. 2004; Zoback et al. 2006) and inferred for other segments of the SAF (Townend and Zoback 2004). Explanations include high pore fluid pressures within the fault zone or the presence of weak minerals on the shear plane. Other authors suggested that mantle-derived fluids migrate through the SAF system into the brittle crust (e.g., Kennedy et al. 1997) or that crustal fluids released from metamorphic processes penetrate the fault laterally (Irwin and Barnes

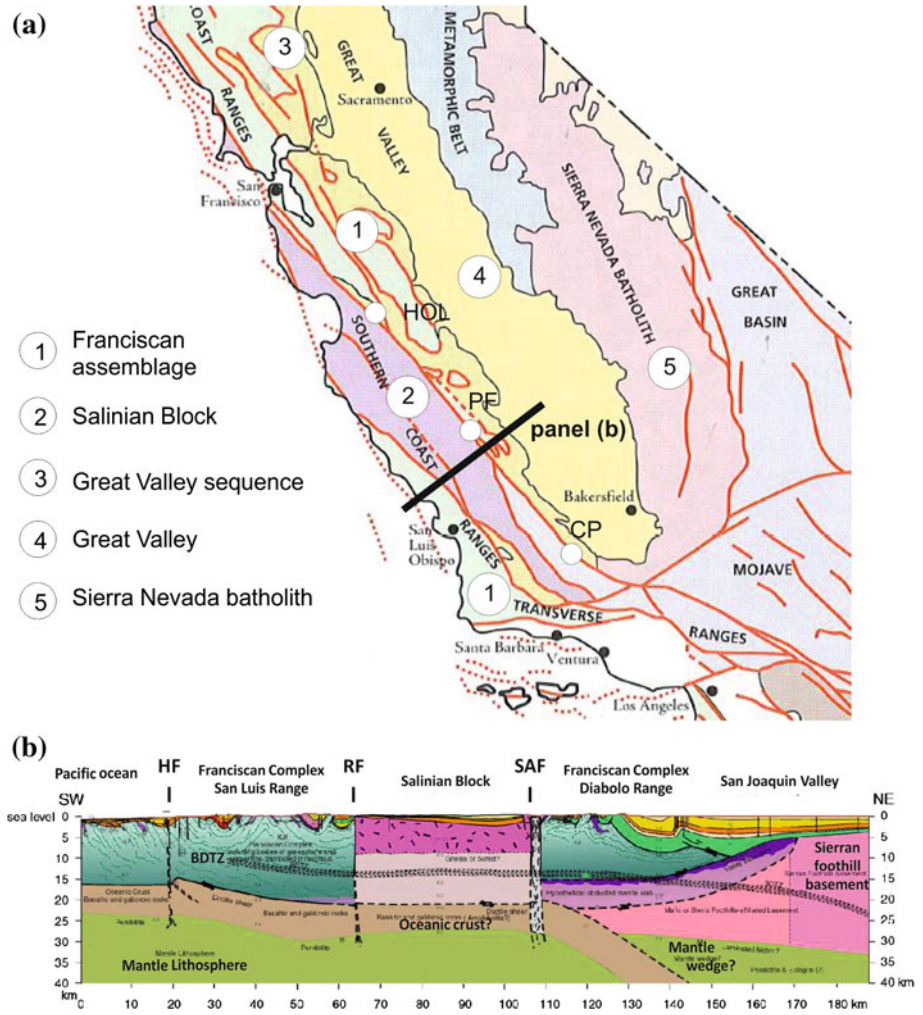

Fig. 2 **a** Simplified map showing the main geological units in central California (*source*: Irwin 1990). **b** Geological cross-section across the Coast Ranges and the SAF near Cholame in central California, based on the compilation of geophysical and geological data by Page et al. (1998) and simplified by Zoback et al. (2002). A rigid block of Salinian granite intervenes between intensively deformed rocks of the Franciscan Formation and is bounded by the SAF to the east and the Rinconada fault, a subparallel strand of the SAF, to the west

1975), thereby contributing to fault-weakening high-fluid pressures (e.g., Rice 1992; Kennedy et al. 1997) and supporting fault creep (Fig. 5c).

Alternatively, or additionally, serpentinite has been suggested to support fault creep, because of its spatial close association with the creeping faults in central and northern California (Fig. 3a). However, serpentinite minerals do not exhibit sufficiently weak shear strengths to account for fault creep. Moore and Rymer (2007) identified talc-filled shears and veins from cuttings of the SAFOD borehole and suggested that interconnected films of talc would only require small volume fractions to attain the observed frictional weakness. Talc, derived as a reaction product from silica-saturated hydrothermal fluids with serpentinite, is

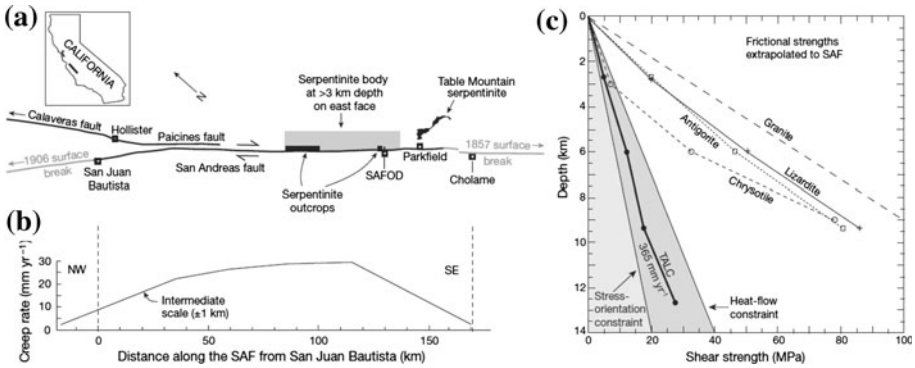

Fig. 3 The potential role of serpentinite for fault creep. **a** Spatial association of serpentinite occurrences along the creeping SAF between San Juan Bautista and Parkfield–Cholame and **b** corresponding creep rates. **c** Shear strength of talc and other minerals versus depth (i.e., pressure). Only talc may account for the inferred low frictional weakness, constrained by stress orientations observed in the SAFOD and by the absence of frictional heat generation. Figures reprinted by permission from Macmillan Publisher LTD: Nature (Moore and Rymer 2007), copyright 2007

frictionally weak over wide pressure and temperature ranges (Fig. 3c); thereby, an indirect link between the occurrence of serpentinite and fault creep is established.

Talc was found in veins and shears which overprint all other textural features in the serpentinite grains. Therefore, Moore and Rymer (2007) proposed that the talc is of recent origin. The chemical reaction of serpentinite with silica-saturated fluids (possibly derived from a deeper fluid source) to talc is a dehydration reaction which releases additional water into the system. However, talc is only a minor constituent of the fault zone rocks ($\sim 0.1\%$), and the associated fluid volumes are probably too small to influence the mechanical behavior of the fault directly. The presence of recently formed talc suggests fluid influx (transporting dissolved silica) into the fault system as well as the occurrence of active dehydration processes in the crust. All explanations for fault creep imply fluid circulation within the fault zone, closely related to or in combination with high-pressure fluids.

2.3 The Fault Zone Conductor

Conceptual fault zone models motivated MT studies to investigate the fluid distribution within and surrounding the fault zone. Early MT studies at Parkfield (Eberhart-Philips et al. 1995), in combination with seismic tomography, and at Carrizo Plain (Mackie et al. 1997) were able to discriminate some major geological units of the SAF system in terms of their electrical properties. In particular, the MT models at Parkfield revealed a distinct upper crustal high-conductivity zone NE of the SAF (Fig. 4a), coincident with a seismic low-velocity zone. This zone was related to high-pore pressure brines, and Eberhart-Philips et al. (1995) speculated that fluids could be forced from the Coalinga anticline region in the NE to Middle Mountain, a push-up structure centered on the SAF near the SAFOD (Fig. 4a). Such a model was consistent with earlier fault zone models (Irwin and Barnes 1975; Eberhart-Philips et al. 1995) predicting that fluids released by metamorphic reactions within the Franciscan formation infiltrate the SAF (Fig. 4b) and generate localized zones of high fluid pressure (Irwin and Barnes 1975; Rice 1992) (see conceptual model by Eberhart-Philips et al. (1995) in Fig. 4b).

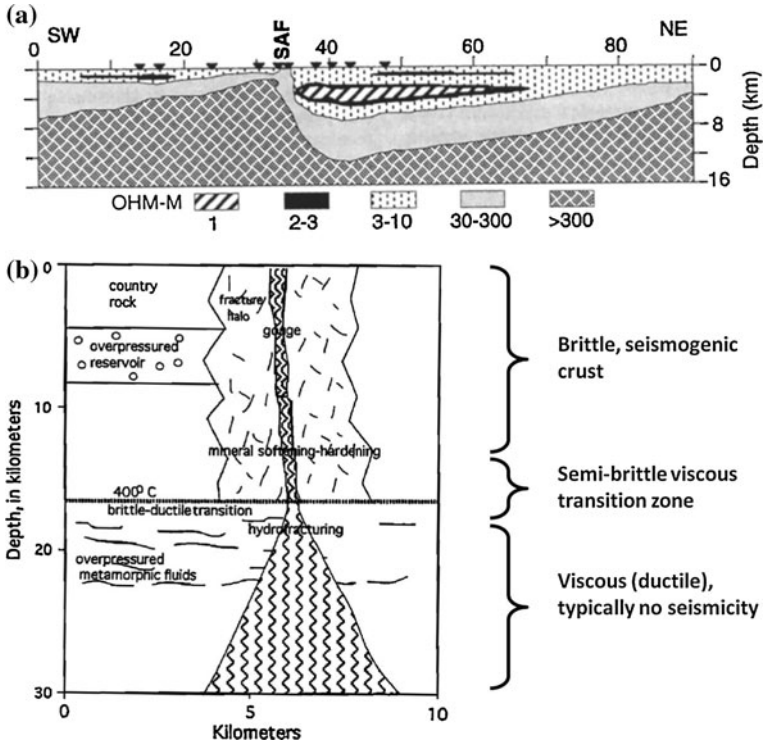

Fig. 4 **a** Resistivity model across the SAF near Parkfield (Eberhart-Philips et al. 1995) and **b** conceptual fault zone model. Low resistivities northeast of the San Andreas were interpreted with the presence of brines. Figures from Eberhart-Philips et al. (1995)

A different situation was encountered at Carrizo Plain, where the upper and middle crust east of the SAF appeared resistive, in contrast to simple geological models which juxtapose resistive Salinian against presumably more conductive Franciscan formations along the SAF (Mackie et al. 1997). These early investigations at Parkfield and Carrizo Plain were limited by spatial sampling distances of 5 km on average, too coarse to resolve electrical structure related to the internal architecture of the SAF (Fig. 6b).

High-resolution MT studies across the SAF with continuous electric field profiling in its central parts revealed a more detailed electrical image of the SAF at Parkfield (Unsworth et al. 1997, 2000; Unsworth and Bedrosian 2004a) and Carrizo Plain (Unsworth et al. 1999) and, later, at Hollister (Bedrosian et al. 2004). All of these studies imaged the upper few kilometers of the fault-surrounding crust. The most prominent feature of these models is a wedge-shaped high-conductivity zone above (Parkfield) or adjacent (Hollister) to the seismically defined fault (Fig. 5). High conductivities in the uppermost portion of the fault were also imaged at Carrizo Plain, but as a less pronounced feature of the resistivity model (Fig. 6a). FZCs, prominently visible at Parkfield and Hollister, and modestly at Carrizo Plain, have been interpreted as saline fluid circulation within the damage zone of the SAF and many other faults worldwide (Ritter et al. 2005; Hoffmann-Rothe et al. 2004). FZCs have been found along the SAF, where the fault exhibits creeps or is in a transitional state, i.e., along two parallel profiles at Hollister and three profiles at Parkfield.

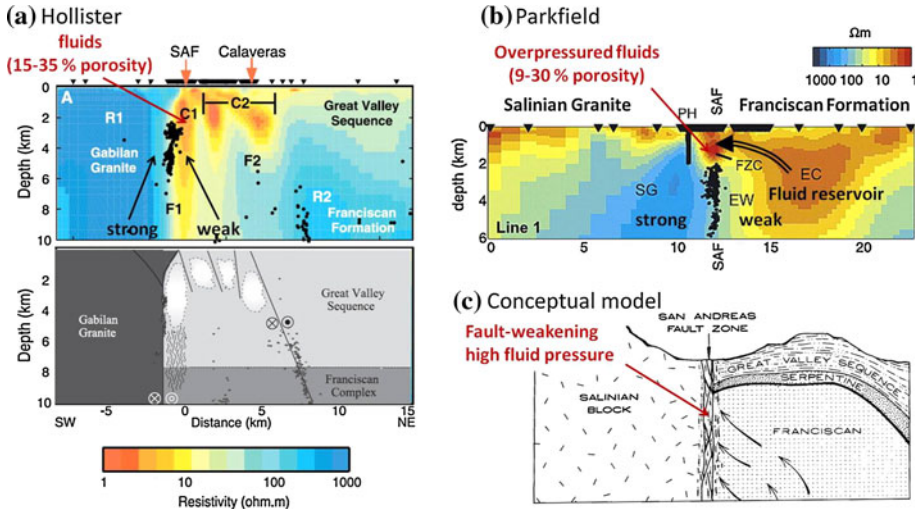

Fig. 5 Upper crustal resistivity models obtained from 2D inversion of MT data **a** near Hollister (modified after Bedrosian et al. 2004) and **b** near Parkfield (modified after Unsworth and Bedrosian 2004a). The magnitude of the fault zone conductor (*FZC*), believed to characterize saline fluids circulating within the damage zone of the fault, is variable along strike and correlates with the fault activity (e.g., Unsworth et al. 1999; Ritter et al. 2005). **c** Conceptual fault zone model of the SAF where it exhibits creep, modified after Irwin and Barnes (1975). Fluids, released by metamorphic reactions within the Franciscan formation and kept at high pressure below an impermeable layer (serpentinite or layers of the Great Valley sequence) migrate laterally into the fault zone. High pressure fluids contribute to fault-weakening and reduce shear strength

Salinities measured in water wells at Parkfield (Hollister) require porosities of 9–30% (15–35%) to account for the observed conductivity within the upper 2–3 kilometers of the fault, based on Archie's law (Bedrosian et al. 2004; Unsworth and Bedrosian 2004a). At both locations, the FZC coincides with zones of reduced seismic compressional wave velocity (v_p) and enhanced v_p/v_s ratios (where v_s is the shear-wave velocity), consistent with a fluid-filled porosity network (e.g., Thurber et al. 2004). Fluid-filled voids and fractures are therefore interpreted to represent the brecciated and damaged zone of the fault (Caine et al. 1996).

At the SAF, the width and depth extent of the FZC varies along strike. At Hollister, where the fault creeps at high rates, the anomalous zone of high conductivity comprises several pockets of high conductivity between the San Andreas and Calaveras faults and extends to mid-crustal depths beneath the SAF (Bedrosian et al. 2004) (Fig. 5a). At Parkfield, where the fault is in transition from creep to fault lock, anomalous conductivity is confined to a zone centered on the SAF and extending from the surface to a depth of 2–5 km (Fig. 5b) (Unsworth et al. 2000). In contrast, the FZC at the seismically quiescent SAF at Carrizo Plain is only weakly expressed, both in terms of conductivity and depth extent (Fig. 6a).

Along-strike variations of the FZC, with the more active fault segments associated with wider, deeper, and more conductive FZCs, provide some insight into how the FZC developed. In a detailed comparative study, Ritter et al. (2005) address the interplay between the extent and conductivity of the FZC, lithology, fluid supply, permeability, and fault geometry. They proposed that the extent of the FZC along the SAF reflects repeated episodes of healing, strength reloading, and subsequent failure, causing the formation of broad zones of structural deformation. They further suggest that a prominent strength contrast across the fault may result in deformation zones which effects the weaker, eastern

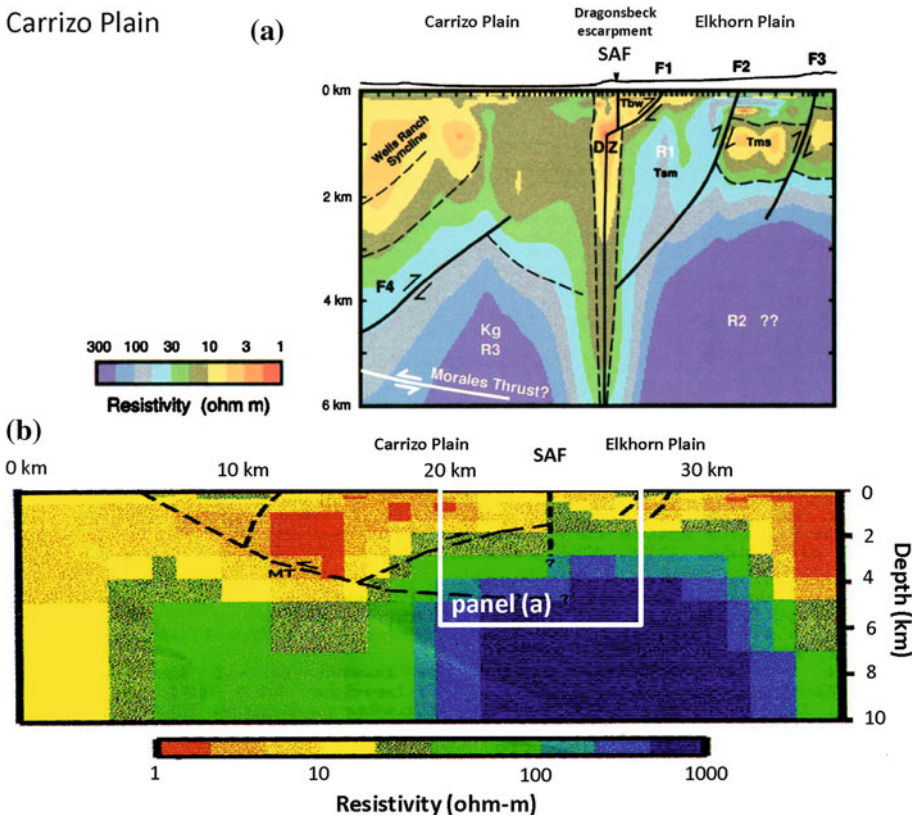

Fig. 6 Resistivity structure at Carrizo Plain. **a** High-resolution MT study imaged a modest FZC; the conductance is significantly less when compared with the creeping segments near Parkfield and Hollister (Unsworth et al. 1999). **b** Upper crustal resistivity structure, showing a competent resistive block beneath and east of the SAF (Mackie et al. 1997). *White rectangle* outlines model section shown in **a**

block over a wider range. This seems to be characteristic for upper to mid-crustal levels of the SAF near Hollister, and also for Parkfield at depths below the FZC.

Highly damaged rocks within the SAF zone at Parkfield form a low-velocity waveguide for seismic waves, giving rise to fault-guided wave propagation (Eberhart-Philips et al. 1995). Using surface and borehole seismic observations, Li and Malin (2008) estimate that a low-velocity waveguide along the fault at SAFOD extends at least to depths of $\sim$7 km and constitutes of a 30–40 m wide low-velocity fault-core embedded in a 100–200 m wide damage zone. The waveguide coincides with the FZC in its upper portion, but can be traced to greater depths. Increasing confining pressure with depth results in reduced porosity (compaction), increasing seismic velocities within the waveguide, and, in conjunction with possible changes in the fluid composition, higher resistivities when compared with the FZC residing within the upper 2–3 km.

Fault zone conductors have been observed at different fault zones, but they are not necessarily associated with all shear zones. At the DST, no fault zone conductor was observed with a high-resolution MT study (Ritter et al. 2005). One possible explanation is that strain may have been localized for a considerable time span along a narrow, meter-scale damage zone, too small to be sensed with MT.

2.4 Seismicity–Resistivity Correlation

It is an intriguing observation that the regions characterized by FZCs are to a large extent devoid of microseismicity. Ritter et al. (2005) pointed out that the spatial relationship between the seismically defined active shear plan and the damage zone of the fault characterized by the FZC sheds some light on the dynamics of faulting.

At Parkfield, the onset of seismicity is at 2–5 km depth, coincident with the base of the FZC. Below the FZC, seismicity is localized between the resistive Salinian basement on the Pacific plate and more conductive rocks comprising the Franciscan formation and sediments of the GVS on the North American plate. At Hollister, the upper 2 km, corresponding to the zone of highest conductivity, is also devoid of seismicity, and seismicity associated with the SAF marks the western margin of the deeper parts of the FZC. The onset of seismicity along the Calavares fault near Hollister is at $\sim$5 km depth and correlates with a sharp increase in resistivity with depth; the connection between the seismically defined Calavares fault and its surface trace penetrates through conductive material and exhibits only minor seismicity (Fig. 5)

The absence of seismicity was used to suggest that the fluid-saturated fault breccias composing the FZCs are too weak to accumulate the shear stresses necessary to undergo brittle failure (Unsworth et al. 2000), provided that fluids are at hydrostatic pressure and hydraulically interconnected (Ritter et al. 2005). In turn, a sharp resistivity contrast across the western edge of the FZCs suggests that the fault is impermeable for cross-fault fluid flow at deeper levels (Bedrosian et al. 2004; Ritter et al. 2005), in agreement with the onset of seismicity and with little geochemical evidence for fluid mixing across the fault. Because fluids at hydrostatic pressure tend to inhibit seismicity and overpressured fluids tend to induce seismicity, the spatial relationship between the FZC and seismicity helps to characterize fluid pressure and permeability distribution within and surrounding the fault.

Fluid-induced seismicity is not specific to the SAF but is also known on a larger scale and from deeper crustal levels. Gürer and Bayrak (2007) compiled a comprehensive catalog describing the spatial relationship between electrically conductive zones and the distribution of seismicity for a number of tectonically active zones world wide. In general, fluid-induced seismicity involves high pressure fluids (sourced in conductive zones) invading rheologically strong (and resistive) formations, thereby facilitating mechanical failure and actively triggering seismicity or earthquakes within critically stressed regions (Jiracek et al. 2007).

Microseismicity along the SAF appears to localize in zones which exhibit a lithological contrast associated with a lateral conductivity gradient or contrast on a kilometer scale, from strong, resistive rocks to weak, conductive material (cf. Fig. 5). Superimposed on this kilometer scale trend is the actually deforming fault. SAFOD observations of the actively deforming fault strands have shown that the fault core (localized on a meter scale) is considerably weaker than its wall rocks. This does not, however, imply that the weak SAF originally developed in a rheological gradient or contrast zone, because the western Salinian block has been displaced along a (pre-existing) fault to its present position. Nevertheless, the inferred rheological heterogeneities surrounding the fault zone may affect the present deformation and should be used to better constrain mechanical models, which are frequently based on layered-earth background rheology models (e.g., Chéry et al. 2004).

2.5 Crustal Fluid Source and Indications for Mantle-Derived Fluids

The source of fluids circulating in the damage zone, and in formations surrounding the fault, is probably multifold. In addition to fluids of meteoric origin, with a maximum

circulation depth of ~6 km (Kharaka et al. 1999) estimated on the basis of geochemical signatures of spring and well fluids, Irwin and Barnes (1975) suggested that fluids emanate from metamorphic reactions within the Franciscan complex. These fluids could be transported laterally into the fault zone, because they are capped by impermeable layers of the Great Valley sequence or a layer of serpentinite (cf. conceptual model in Fig. 5c). Geochemical studies of fault zone materials by Pili et al. (1998) support this conclusion and suggest that, during deformation, the fault zone is infiltrated by mixed H_2O–CO_2 fluids of metamorphic or deep crustal origin. Finally, a locally high flux of mantle-derived fluids is inferred by Kennedy et al. (1997) based on helium isotopic ratios in springs and seeps along the SAF.

Kennedy et al. (1997) proposed that a permeable fault or damage zone surrounded by low-permeability country rock may act as a conduit for mantle-derived fluids and allow for large fluid pressures to be localized within the fault zone (Rice 1992). They argued that mantle fluids passing through the ductile lower crust must enter the brittle fault zone at or near-lithostatic pressures and suggested that they may thus contribute directly to fault-weakening high-fluid pressures at seismogenic depths.

However, SAFOD observations, including contrasts in both fluid chemistry and fluid pressure across the fault zone, suggest that, rather than acting as a permeable conduit, the fault appears to be considerably less permeable than the surrounding crust and acts as a barrier for both vertical and horizontal fluid flow (Zoback et al. 2006). This would be in agreement with a sharp resistivity contrast across the seismically defined fault, as observed near Hollister and, at depths below the FZC, near Parkfield (Fig. 5). Furthermore, SAFOD provided no evidence for near-lithostatic fluid pressures within the fault core. Zoback et al. (2010) thus concluded that high fluid pressures are not the primary cause for the apparent weakness of the fault.

However, observations at the depth of the SAFOD borehole may not fully reflect the fluid pressure state within the fault zone over much of its depth extent. It can therefore not be precluded that the fault is permeable at deeper or shallower levels, that substantially higher fluid pressures exist within deeper portions of the fault (Fulton and Saffer 2009), or that dynamic fluid pressure buildup and pressure release associated with the seismic cycle occurs. However, dynamic changes related to the fluid budget would probably have a minor effect on bulk electrical resistivity, because telluric and MT monitoring did not detect any resistivity changes which could be associated with the Parkfield M6.0 earthquake (Park et al. 2007; Kappler et al. 2010).

It has furthermore been observed that fluid pressures and mantle-derived gas concentrations are elevated within the fault-adjacent country rock of the North American plate. Additionally, geochemical signatures of mud gas, logged while drilling the SAFOD (Wiersberg and Erzinger 2007), revealed a positive mantle-derived gas concentrations gradient away from the SAF into the North American plate, suggesting that pathways exist adjacent to the fault and that deeply sourced fluids may percolate into the eastern fault block.

The upper crustal lithology east of the SAF near Parkfield comprises both sediments from the Great Valley Sequence and Franciscan Formation. Within this geology, a pronounced zone of high electrical conductivities (Eberhart-Philips et al. 1995; Unsworth and Bedrosian 2004a; Becken et al. 2008), coincident with a region of lowered velocities (Thurber et al. 2004), may represent the source or a trap for crustal and mantle-derived fluids which are speculated to penetrate the fault zone laterally from the east (Unsworth and Bedrosian 2004a). This zone is referred to as the eastern conductor (EC). In this region, a 2 km deep layer of magnetic serpentinite is interpreted from potential field data

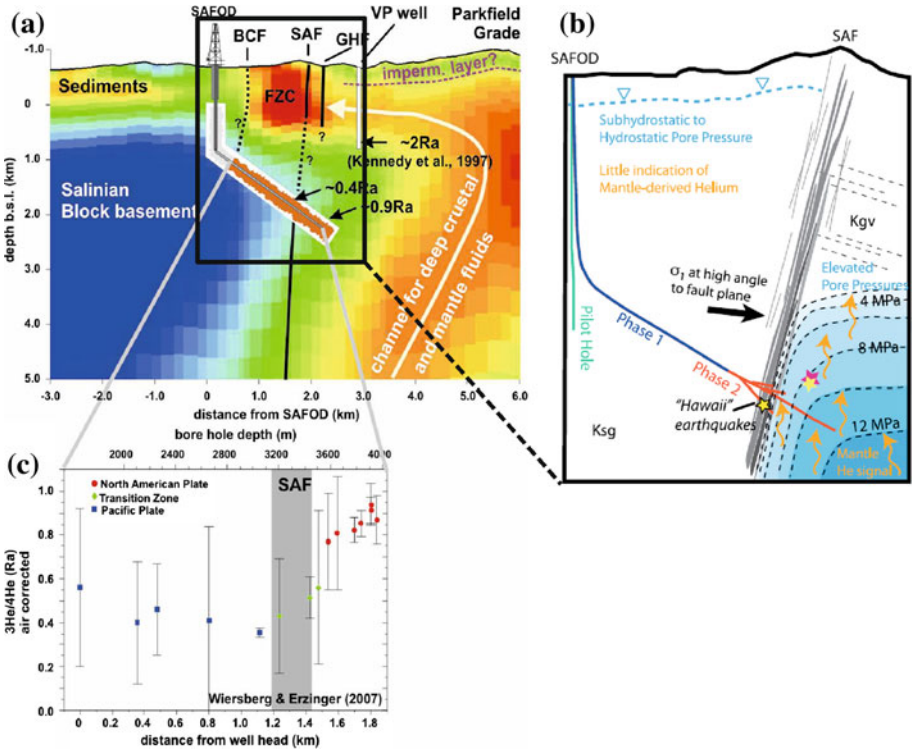

Fig. 7 Scenario for fluid distribution in the vicinity of the SAFOD, with influx from mantle-derived fluids. **a** Resistivity model across the SAFOD (Becken et al. 2008) coincident with *line 1* of Unsworth and Bedrosian (2004a) shown in Fig. 5a. **b** Predicted fluid pressure distribution in the North American Plate due to dehydration of a serpentinized mantle wedge (Fulton and Saffer 2009), which is consistent with SAFOD observations. **c** A profile of $^{3}He/^{4}He$ ratios across the SAF indicates increased mantle-derived gas concentration within the North American plate (Wiersberg and Erzinger 2007), consistent with earlier He isotope studies in the Varian Philipps (*VP*) water well (Kennedy et al. 1997). Suprahydrostatic fluid pressures within the North American Plate, He isotope studies and the MT resistivity model agree in suggesting that pathways for deep fluids exist into the North American plate and that fluids are trapped between an impermeable SAF and an impermeable near-surface layer

(McPhee et al. 2004); however, it remains unconfirmed from MT data (Unsworth and Bedrosian 2004a). Such a layer of serpentinite, or layers of the GVS, could act as an impermeable seal, as suggested by Irwin and Barnes (1975), and give rise to overpressured fluids within the reservoir below and consequently drive fluids laterally toward the fault zone.

Lateral fluid flow from the east into the fault requires open pathways between the EC and the seismically defined fault itself. The geometry of these pathways, if existing, is, however, not clear. Seismic joint v_p, v_s and $v_p v_p/v_s$ inversion (Zhang et al. 2009) and seismic attenuation tomography (Bennington et al. 2008) consistently infer a fault-adjacent near-vertical zone that is characterized by high v_p/v_s ratios and low attenuation. This anomalous zone easterly adjacent to the fault extends below $\sim$1 km depth, is less than 1 km wide, separates the FZC region (characterized by low resistivity and low velocity) from the EC, and appears to coincide with a sliver of GVS sediments (cf. Figure 7f in Zhang et al. 2009). Its seismic properties are indicative of a low-porosity zone and do not

support the previous MT interpretations of fluid pathways into the FZC at these depth levels (Unsworth and Bedrosian 2004a). Potential fluid flow into the FZC is therefore more likely concentrated at shallower levels, coincident with the zone of highest conductivities in the upper 1 km (cf. sketched fluid path in Fig. 7a), and possibly at deeper levels.

The situation may be different at Hollister, where GVS sediments are based on the moderately resistive Franciscan Formation at 6–8 km depth, and where a fluid source or reservoir within the fault-adjacent rocks appears absent. If crustal fluids derived from metamorphic reactions within the Franciscan formation, or fluids of deeper origin, contribute significantly to the fluid budget of the SAF at Hollister, they would possibly migrate along near-vertical pathways easterly adjacent to the SAF, where high conductivities are encountered to mid-crustal levels. At Carrizo Plain, no indications have been found for deeply penetrating conductor zones. Here, the crust appears overly resistive to mid-crustal levels, suggesting that fluid influx from the lower crust or deeper is absent. However, regional-scale MT studies, which could test for the presence or absence of crustal scale conductive zones, are missing from both locations, Hollister and Carrizo Plain.

In summary, SAFOD observations and MT resistivity studies near Parkfield consistently infer deeply rooted fluid pathways into the eastern fault block. Consequently, these results strongly support the existence of a deeper fluid source and at least episodically open pathways for fluids migrating into the brittle regime. However, it remains a debated question, if and how these fluids control the mechanical state of the seismogenic fault.

2.6 Crustal Fluid Pathways

A crustal MT study across the SAF at the SAFOD showed that the EC inferred to be a fluid reservoir or trap for crustal and mantle-derived fluids is rooted in the lower crust or deeper (Fig. 8a). This near-vertical zone of high conductivities, appearing uninterrupted from the near surface east of the fault across the SAF at mid-crustal levels and broadening beneath the SAF into the lower crust, has accordingly been interpreted in terms of a channel for deep fluids into the seismogenic zone (Becken et al. 2008). If explained with interconnected pathways for fluids, and fluid upflow across the entire crust, this conductive channel is consistent with many of the surface and SAFOD observations mentioned above.

Superimposed on the resistivity model in Fig. 8a are structural interpretations from a seismic reflection and refraction survey (Hole et al. 2004; Ryberg et al. 2005; Bleibinhaus et al. 2007; Buske et al. 2007), which show good agreement with the resistivity structure. On the Pacific plate, the Salinian block basement is based on a layer with lowered velocity, interpreted as metasedimentary rocks, and coincident with lowered resistivities here. A near-vertical fault zone (F) imaged with Fresnel-volume-migration (Buske et al. 2007) could correspond to the deep-reaching lateral resistivity contrast at the transition to the Salinian block to the west. An active thrust fault east of the fault that abuts the SAF at the base of the seismogenic zone has been proposed near the edge of the upper crustal high conductivity zone in the upper crustal eastern fault block (EC), based on the analysis of earthquake data (dashed line T in Fig. 8a). The reflector element H (Bleibinhaus et al. 2007) may represent a lower crustal continuation of this thrust.

High-conductivity zones imaged with MT near SAFOD appear in spatial close association with the occurrence of serpentinite, and could be causally or indirectly related. Evidence for widespread serpentinite occurrence comes from nearby outcrops, in combination with aeromagnetic interpretation, and serpentinite and talc findings within SAFOD (cf. Sect. 2.2). Serpentinite originates from ultramafic mantle rocks which have been altered by hydration. Serpentinite is weaker than unaltered mantle peridotite, exhibits more viscous mechanical

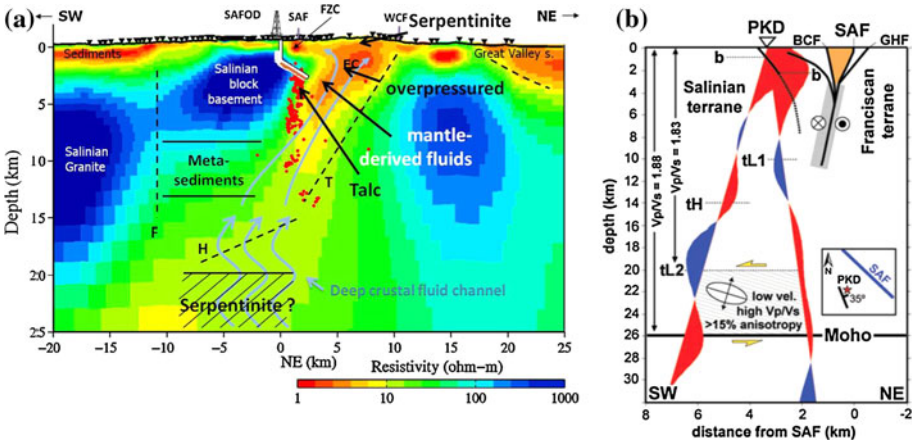

Fig. 8 Crustal structure at SAFOD. **a** Interpreted MT resistivity model. High electrical conductivities appear uninterrupted from the EC into the lower crust or deeper and have been proposed to represent pathways for fluids (Becken et al. 2008), consistent with elevated fluid pressures and mantle-derived fluid concentrations in the eastern fault block. A seismic low-velocity layer below the resistor denoted as the Salinian block basement, and a reflector element (*H*) have been interpreted from a seismic reflection experiment (Bleibinhaus et al. 2007). *T* may represent a thrust fault (Carena 2006), bounding the zone of highest electrical conductivities to the east. *F* indicates a fault zone illuminated by Fresnel-volume-migration of the same seismic data set (Buske et al. 2007). *Red dots* mark seismicity. **b** Polarity reversal of receiver functions at station PKD located above the Salinian block have been modeled with an anisotropic layer, possibly corresponding to serpentinite (Ozacar and Zandt 2009); we propose that the zone imaged as electrically conductive may correspond to the exhumation path for serpentinite (see text)

properties and lower density. Due to its buoyancy under high confining pressures at depth, serpentinite is prone to exhumation through weak zones in the crust. Kirby et al. (2002) suggested that a serpentinized mantle wedge, relic from ceased Farallon subduction, may be a deep source region for serpentinite slivers that occur along the SAF. If this was the case, it would be possible that remnants of serpentinite exist also at deeper crustal levels.

A recent receiver function (RF) study supports the occurrence of serpentinite within the lower crust (Ozacar and Zandt 2009). Using data from a long-term seismological station (PKD) located 3 km SW of the SAF near SAFOD, Ozacar and Zandt (2009) found that RFs display strong polarity reversals that require strong seismic anisotropy in a low velocity, high v_p/v_s layer at 18–26 km depth, that has a ENE dipping rock fabric (Fig. 8b). The authors suggested that serpentinite at lower crustal pressure conditions could exhibit the modeled low velocity and high v_p/v_s ratio simultaneously; other rock types are typically faster or have lower v_p/v_s ratios, even if fluid bearing. The orientation of ENE anisotropic fabric of this layer, dipping at only 35°, is inconsistent with the San Andreas sense of shear. Therefore, Ozacar and Zandt (2009) explained the anisotropic layer with a fossilized fabric of past eastward-directed (Farallon Plate) subduction, maintained in serpentinite rocks. Ozacar and Zandt (2009) suggested that their finding is of regional significance, because they found similar patters in RFs evaluated in southern California; however, no additional RF has yet been analyzed in central California.

Receiver functions place the presumed serpentinite layer at the base of the crust to the southwest of the seismically defined SAF, probably owing to the position of the PKD site west of the fault. However, a serpentinite sliver at depth located west of the fault trace

would be in geometrical agreement with an overall SW dipping geometry of the crustal conductor inferred to represent pathways for fluids.

Based on the coincidence of conductive zones and serpentinite at different crustal levels, we hypothesize that the crustal conductive zone coincides with a region occupied by serpentinite slivers, and that fluid pathways are related to the crustal exhumation path of serpentinite. Fluids (episodically) migrating along these pathways could contribute to elevated fluid pressures and explain elevated mantle-derived gas observed within the SAFOD on the North American plate (Wiersberg and Erzinger 2007) and within nearby water wells (Kennedy et al. 1997; Zoback et al. 2006) and could furthermore provide dissolved silica reacting with emplaced serpentinite to talc (Moore and Rymer 2007) (cf. Sect. 2.2)

If crustal pathways for fluids are spatially related with the exhumation path of serpentinite, and if RFs can probe for serpentinite at lower crustal levels, as proposed by Ozacar and Zandt (2009), then the combination of MT and RF analysis could be useful to determine systematic variations of crustal conductive zones, serpentinite occurrence at depth and their relationship to the mechanical state of the fault. Unfortunately, the PKD station is the only station nearby Parkfield, which provided long enough recordings to apply this analysis (A. A. Ozacar, personal communication).

Deformation in shear zones can also generate electrical anisotropy. Bedrosian et al. (2004) reported about three-dimensional effects in their MT data acquired across the SAF near Hollister. For the purpose of two-dimensional inversion, they had omitted the longest period range in their data. However, based on anisotropic forward modeling, Bedrosian and Unsworth (2003) suggested that models containing an anisotropic ductile shear zone can account for the observed three-dimensional behavior of observed induction vectors at Hollister. This explanation implies that electrical anisotropy has developed in response to ongoing strain along the deeper roots of SAF and could thus be characteristic also for other portions of the fault (Jiracek et al. 2007). Electrical anisotropy in shear zones warrants further investigation, and the San Andreas is a promising target to study this and its relationship to deformation and to structural heterogeneities at different depth levels. However, it is difficult to separate effects arising from the nearby ocean, structural heterogeneities across the fault, local three-dimensionality and anisotropy (Unsworth and Bedrosian 2004b).

2.7 Fluid Migration Across the Brittle-Ductile Transition Zone

Fluid flow through rocks at different crustal and upper mantle depths has received considerable attention during the last decade. In general, fluids are driven upward owing to buoyancy forces acting on low-density fluids. However, upward crustal fluid flow may become arrested at mid-crustal levels, and uninterrupted fluid pathways across mid-crustal levels seem to be the exception rather than the rule. Different mechanisms and models are invoked to explain fluid flow and fluid arrest. Understanding fluid flow patterns from a thermomechanical perspective is beyond the scope of this paper. However, as it is anticipated that mantle-derived fluids percolate into upper crustal fault blocks, we briefly summarize some aspects of fluid flow through the crustal levels.

According to modern thermomechanical models, under compressional conditions even initially pervasive pore fluids are mechanically unstable and must form focused flows whose shape depends on the relations of fluid and lithostatic pressures (e.g., Connolly and Podladchikov 2004). Porosity waves are one of the possible mechanisms for both segregation and trapping of fluids released by diagenetic and metamorphic reactions. Ascending

buoyant fluids are envisaged as percolating upward through an interconnected fluid-filled porosity network. Flow can become pulsed in zones of high porosity, may grow by draining fluid from the background porosity and leave a wake of elevated porosity that localizes subsequent flow.

Porosity waves may be stalled below a high-strength layer or in stagnant zones of tectonically induced neutral buoyancy (Connolly and Podladchikov 2004). These mechanisms can result in the formation of high pressure fluid reservoirs below the transition between the brittle and ductile portions of the crust. Jiracek et al. (2007) explore these concepts to address the question of how earthquake rupture in the brittle crust is initiated by permeable, overpressured fluidized zones in the ductile crust. Evidence for the existence of stalled fluids (both melts and aqueous fluids) below the brittle-ductile (BD) transition zones comes from MT studies around the world, which frequently imaged lower crustal high conductivity with clear depth to their top below the BD transition or deeper.

The situation seems to be different at the SAF near SAFOD, where a subvertical zone of high conductivities occurs in the ductile crust beneath the SAF and appears to continue uninterrupted to the near surface. Comparing these results with MT models from the Himalayas and from New Zealand, Jiracek et al. (2007) pointed out that untapped and continuously rising fluids may facilitate weaker but more frequent earthquakes compared with the Southern Alps in New Zealand and the Himalayas. They suggested that low convergence characterizing the Coast Ranges in central California rates may not allow the formation of stalled fluid reservoirs in stagnant regions of neutral buoyancy or at permeability or strength contrast, because their formation is favored in compressional settings.

In addition to these explanations, we note that the crustal conductive zone has oblique, apparently westward dipping geometry, and breaches the BD transition zone at the base of seismically defined fault. As pointed out previously, the SAF is an extremely weak zone, is associated with stress rotation, and may perturb the depth range of tectonically induced neutral buoyancy or even prevent its formation in its vicinity. Thus, the concept of fluid stalling and the formation of high pressure regions at mid-crustal levels may not be applicable to the particular, highly heterogeneous situation at the SAF near the SAFOD, and continuously or episodically open pathways for fluids across the BD transition do not contradict the concept of neutral buoyancy in general.

Furthermore, as we shall see later, a high-conductivity zone with its top clearly located below the BD transition was found beneath the Coast Ranges, offset from the SAF to the west, and could indeed correspond to stalled fluids as promoted by the concept of tectonically induced neutral buoyancy.

3 The Deeper Roots of the SAF, Fluid Sources and Geodynamic Implications

The deeper roots are less amenable to direct observation of fault activity, and different models for the deep roots of fault zones such as the SAF have been proposed. Endmember models include distributed upper crustal strain rooted in a broad ductile shear zones, singular through-going faults, or upper crustal faults connected via mid-crustal decollements, and have been discussed in Ritter et al. (2005).

Tectonic Non-Volcanic Tremor (NVT), a recently discovered seismic signal (Nadeau and Dolenc 2005) is believed to provide new insight into the geometry and physical conditions of the deep roots of faults. NVT observations at the SAF system are confined to a small number of source regions, probably limited by detection threshold. Highest tremor activity is observed near Cholame, at the northern end of the zone that was last ruptured by

the Fort Tejon earthquake in 1857 (Nadeau and Dolenc 2005). Because the nucleation of tremor is believed to be intimately related to fluids, we start the discussion of the deeper roots of the SAF with recent NVT observations. We will then expand the discussion by including results from a regional-scale MT survey in the tremor source region and consider implications for the geodynamic setting.

3.1 Non-Volcanic Tremor (NVT)

Accurate localization of tremor is generally difficult because of the absence of a sharp onset of seismic energy for this family of signals. Most authors have located tremor vertically beneath the SAF at depths greater than 25 km (Nadeau and Dolenc 2005; Shelly et al. 2009). The localization techniques used by these authors estimate tremor sources relative to some master event, which yields high relative localization accuracy, but may be biased due to inaccuracies in the master event position. Alternative location estimates are based on the analysis of data from so-called small seismic aperture arrays (SSAA), which determine absolute source positions for each individual tremor episode. Using this approach, Ryberg et al. (2010) determined source locations at slightly greater depths (30–50 km) and systematically offset from the SAF by 15–20 km. Epicenters estimated with both techniques are indicated on the map in Fig. 9. To match the source locations of Shelly et al. (2009), a calibration technique was applied to the SSAA estimates. However, the discrepancies show that there remains some uncertainty about the exact source region of tremor near Cholame.

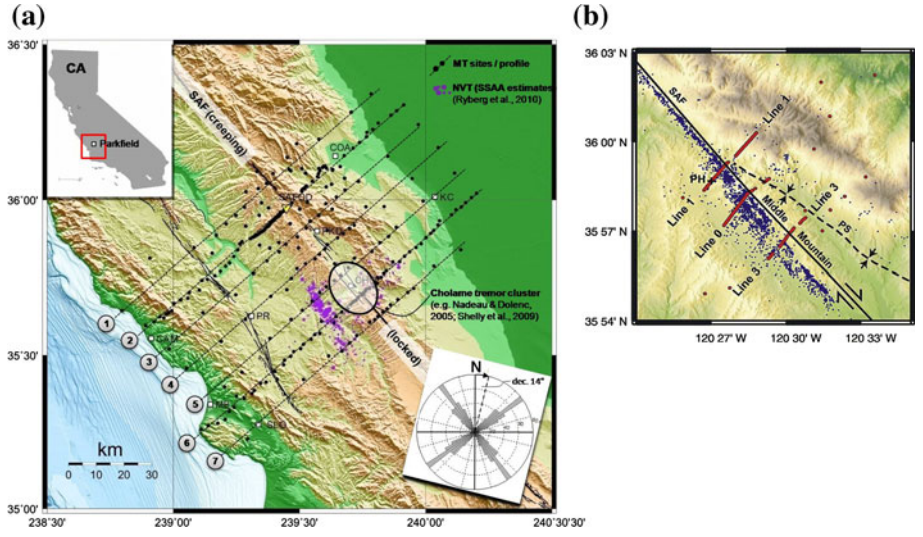

Fig. 9 MT sites probing upper mantle and crustal structure along the Parkfield–Cholame segment of the SAF in central California. **a** Regional-scale MT study (Becken et al. 2011) using seven 120–140 km long profiles. *Black dots* depict MT site locations. *Rose diagram* in the lower inset displays cumulative geoelectric strike estimates consistent with the geological strike of the SAF. *Purple dots*: NVT epicenter estimates based on the SSAA technique (Ryberg et al. 2010); *Shaded ellipse*: outline of NVT epicenters, based on other localization techniques (Nadeau and Dolenc 2005; Shelly et al. 2009); *Black rectangle*: outline of the map section shown in *right panel*. **b** High-resolution investigation of the SAF (Unsworth and Bedrosian 2004a). *Red dots* indicate MT stations; *blue dots* show seismicity. *PH SAFOD* pilot hole, *PS* Parkfield syncline. An additional dense MT profile farther south is beyond the map extent

Tremor sources are not static but can be shown to migrate along the fault with velocities in the range 17–80 km/h. Tremor has been observed to migrate up to 25 km along the fault, though most of the observed episodes travel by 5–10 km (Shelly 2010). Detailed inspection of along-strike tremor migration episodes has been used to suggest that the fault exists as a (piecewise) continuous structure at the 25 km depth of the investigated tremor families (Shelly 2010).

The source mechanism of NVT is not well understood. High pore fluid pressures, released by dehydration reactions in the subducting plate, have been suggested to promote the nucleation of deep NVT, low-frequency earthquakes and slow-slip at the Cascadia subduction zone (Schwartz and Rokosky 2007) and in Japan (Shelly et al. 2006). In subduction zones, these seismic phenomena appear to represent a mode of failure along the subducted plate interface between the locked megathrust updip and the continuously creeping zone downdip (e.g., Obara 2002).

Teleseismic triggering and tidal forcing of NVT at the SAF near Cholame and at other locations indicates that the deep fault is extremely sensitive to small stress perturbations. This suggests the presence of high, near-lithostatic fluid pressures in a critically stressed source region (Thomas et al. 2009), similar to the physical conditions proposed for subduction zone tremor. High fluid pressures may make the fault extremely weak, possibly permitting patches of the deep fault to deform by brittle rather than ductile failure, and support localized slip on the deep extension of the SAF (Shelly 2010). Localized deformation in the ductile deformation region is possible where strain softening occurs and water-weakening is one mechanism to facilitate this (Jiracek et al. 2007). Thus, tremor occurrences provide several indirect indications for the existence of a fluid source at tremor source depth.

The nature of the fault between the base of the seismically defined fault ($\sim$15 km) and the onset of tremor ($\sim$24 km, or deeper), however, is unknown, as this area is devoid of earthquakes and does not appear to generate measurable tremor. Nadeau and Dolenc (2005) found that changes in tremor and micro-earthquake rates at Cholame appear to correlate. This suggests that deep deformation associated with the Cholame tremors may also be stressing the shallower seismogenic zone in this area. In turn, tremor rate and recurrence behavior changes in the wake of the 2004 M6.0 Parkfield earthquake may reflect the effects of static and dynamic stresses imparted by the earthquake and influencing ongoing deep fault deformation. These examples show that tremor on the deep fault and seismicity and earthquakes on the upper crustal fault are processes that are coupled across lower and mid-crustal levels, suggesting that the fault is throughgoing.

3.2 High-Conductivity Zone in the Lower Crust and Upper Mantle

A regional-scale MT array imaged crustal and upper mantle resistivity structure across the entire transitional Parkfield–Cholame segment of the SAF, from the Pacific coast into the Central Valley. The resistivity models presented in Fig. 11 (Becken et al. 2011) rely on 2D inversion techniques of seven individual profiles constituting the array (Fig. 9a). These models indicate that the across-strike resistivity structure is not uniform along the SAF but exhibits significant along-strike variations. Because of this fact, the validity of a 2D approach may be questioned. Therefore, before discussing the resistivity models, we briefly summarize how 3D effects in the data were taken care off and how the pseudo 3D model (i.e., stitched 2D models) was validated.

Multi-period single-site galvanic distortion and strike analysis (Becken and Burkhardt 2004) of the entire impedance data set yielded strike estimates consistent with the general strike direction of the SAF and the lithological units forming the Coast Range geology (see inset in Fig. 9a). Closer inspection of the data revealed that 3D characteristics are

minimized in this rotated coordinate system but do not vanish for a range of sites. The estimated strike direction is the dominant direction contained in the impedance data, but not necessarily a valid strike direction for all sites. Furthermore, the orientation of induction vectors deviates significantly from the strike-perpendicular profile directions. Therefore, data with obvious 3D effects were downweighted for 2D inversion by imposing error bars in proportion to their departure from 2D characteristics, following the procedure discussed in Becken et al. (2008). This approach helped to avoid overfitting the data where they are afflicted with 3D effects.

To validate the models after 2D inversion, Becken et al. (2011) computed model responses from a 3D model constructed by inter- and extrapolation of 2D models onto a 3D grid. Figure 10 compares 3D modeled with observed induction vectors for a period of $T = 128$ s, corresponding to crustal penetration depths where 3D effects are most prominent. This test shows that the 2D approach can reproduce the most important inductive 3D effects, suggesting that the along-strike variations encountered by 2D techniques are, to some extent, real. Ultimately, 3D inversion will be required to translate all aspects of the 3D data into model structure (Tietze et al. 2010).

Figure 11 shows 2D inversion results along profiles 1–7. Models have been truncated at the profile ends and at 60 km depth. Superimposed on the models are the 3D distributions of seismicity (red dots) and NVT estimates (purple dots) based on the SSAA technique (Ryberg et al. 2010). Profiles 2 and 5 across the SAFOD and the source region of tremor, respectively, are shown in Fig. 12.

The most prominent structure revealed by the MT data is a deep high-conductivity zone (HCZ, 1–5 ohm-m), centered 30–40 km southwest of the SAF below 20 km depth, and elongated in parallel to the SAF. Becken et al. (2011) proposed that mineralized fluids within a interconnected porosity network could account for the observed conductivities of the HCZ centered at 25–30 km depth between the SAF and the coast. Bulk rock conductivity of a multi-phase system is strongest depending on the conductivity of the most conductive phase and its interconnection. Aqueous fluid conductivity is controlled by electrolytic concentration and temperature. Modeling of the Coast Range Heat flow anomaly suggest temperatures of ~ 800°C at 30 km depth near Parkfield (Sass et al. 1997). At these temperatures, the electrical conductivity of sea water is approximately ten times

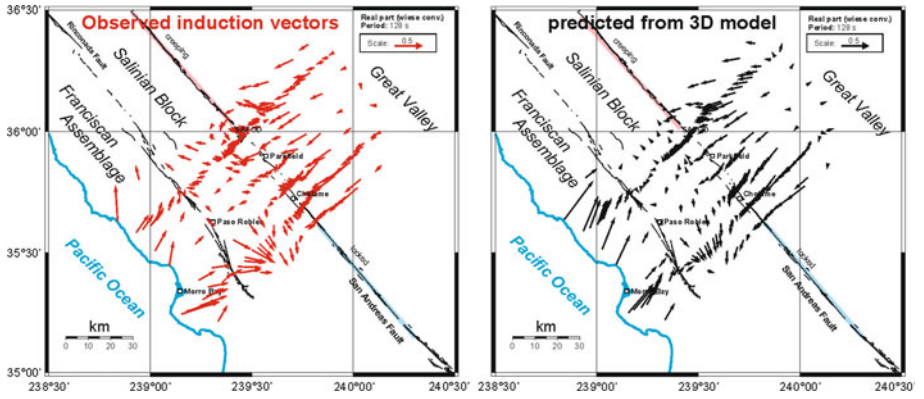

Fig. 10 Comparison of observed induction vectors (real parts, depicted in Wiese convention Wiese 1962) and 3D forward model response, based on inter- and extrapolation of 2D inversion models onto a 3D grid. Period is $T = 128$ s, corresponding to mid-to-lower crustal penetration depth

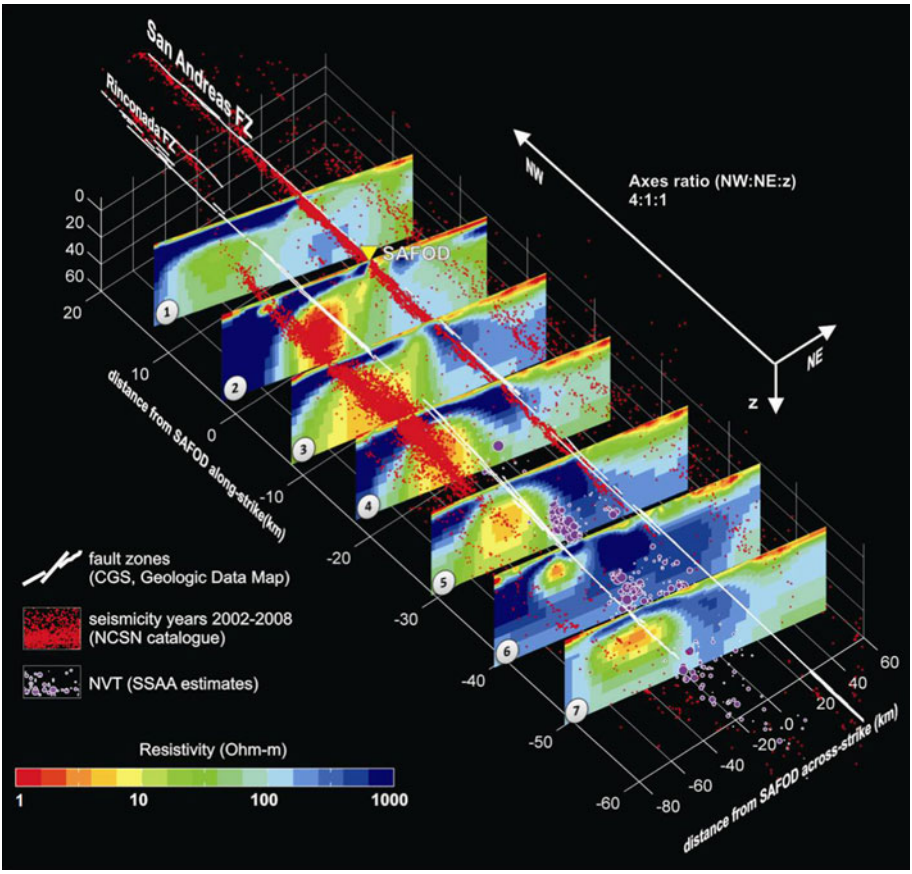

Fig. 11 Regional-scale resistivity structure across the Parkfield–Cholame segment of the SAF in central California obtained from two-dimensional inversion of seven individual 120–140 km long profiles across the SAF (modified after Becken et al. 2011). Models are truncated at 60 km depth. A prominent high-conductivity zone centered at 20–30 km depth and located between the SAF and the coast is interpreted with hydrothermal fluids residing within a strain-generated permeability structure. Crustal fluid pathways have been proposed to account for the conductive crustal zone near the SAFOD, where the SAF is transitional-to-creeping. Farther south, where these pathways are absent, where the brittle fault is transitional-to-locked, and where NVT is observed at depths greater than 20 km, deep fluids may be trapped at high pressures

higher than at room temperatures (Quist and Marshall 1968). Fluids with a salinity comparable to that of sea water and at 800°C have a conductivity of 30 S/m. The Hashin–Shtrickman upper bound (Hashin and Shtrikman 1962) for a two-phase system composed of a resistive rock matrix (0.01 S/m) and a conductive fluid phase (30 S/m) requires 3 vol.% of perfectly interconnected porosity over a large volume to yield bulk conductivities of 1 S/m. A lower degree of pore interconnection would mean larger fluid volumes, which appear unrealistic at these depths. In turn, lower volumes of fluid would be required at the same high degree of interconnectivity if the temperatures and/or the fluid conductivity were higher. Therefore, volumetric porosities as low as a few percent with pores interconnected over large scales are sufficient to explain the observed conductivities of the HCZ.

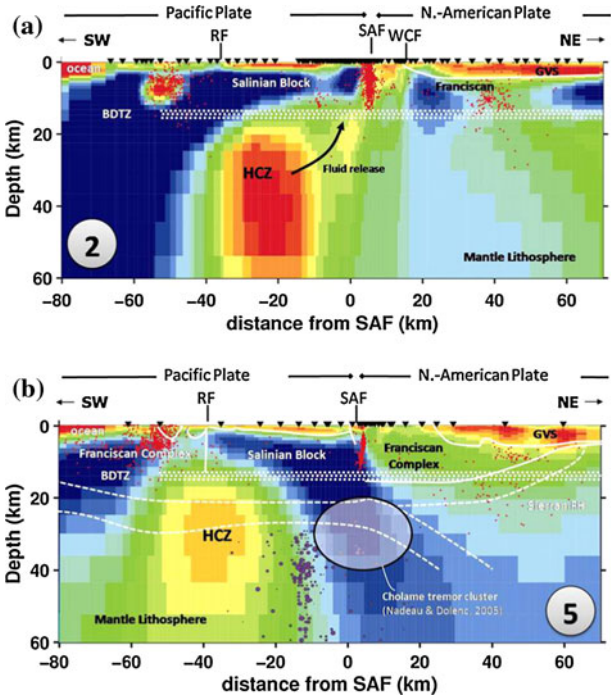

Fig. 12 Regional-scale resistivity models across the SAF **a** at SAFOD near Parkfield **b** at the source region of tremor near Cholame. Models are based on 2D inversion of profile data; the profiles are separated by ~30 km. *Red dots* mark seismicity, *purple dots* indicate NVT source estimates using the SSAA technique Ryberg et al. (2010), ellipse outlines source locations estimated with other techniques (Nadeau and Dolenc 2005). *RF* Rinconda fault, *WCF* Waltham canyon fault, *HCZ* high-conductivity zone, *BDTZ* brittle-ductile transition zone. Superimposed are geological units (*white lines* in **b**) from the coincident geological cross-section depicted in Fig. 2. Resistivity models are the same as in Becken et al. (2011)

Various mechanisms have been discussed for fluid interconnectivity in ductile regimes. These include fracture interconnectivity, grain-edge interconnectivity, or both (Jiracek et al. 2007). In addition, permeability must be maintained over time, either by continuous deformation, permeability-enhancing reactions or high fluid pressures, or a combination of these mechanisms (Jiracek et al. 2007; Cox 2005). Long-lasting deformation can generate interconnection on long distance ranges. A strain-generated porosity network maintained over time could thus explain the degree of pore connectivity assumed by the Hashin–Shtrickman upper bound. Because the actively deforming transform margin migrated inland since its initiation, it is likely that a wide region, from the coast to the fault, has experienced strain during the evolution of the fault system. MT cannot distinguish between permeability structure in actively deforming zones and permeability formed in previously active zones. Only small strain rates, perhaps in combination with other mechanisms, are required to maintain permeability in a ductile deformation regime, once developed (Jiracek et al. 2007). Thus, the HCZ likely represents a ductile deformation region with long-lasting hydraulic permeability.

Note that the HCZ is offset from the SAF and located beneath the predominantly resistive crustal Salinian Block. The Salinian Block is rheologically strong and impermeable for fluid flow in the brittle crust. Below the BD transition, ductile deformation

prevails. Under these circumstances, a stagnant zone of neutral buoyancy could have developed beneath the Salinian Block (deeper than the BD transition) in response to a regional transpressive stress regime. This zone could support the formation of tabular water sills as suggested by Connolly and Podladchikov (2004) and described by Jiracek et al. (2007). Lateral fluid flow in a stagnant zone with small or vanishing vertical hydraulic gradient could be one of the means to drive fluids into the SAF system farther to the east. At the SAF, perturbations in the stress state, associated for instance with a weak fault, and variations of the depth of the BD transition across the fault (Fulton et al. 2010) could result in perturbations of the stagnant zone and facilitate fluid flow further upward across the BD transition zone (cf. Sect. 2.7).

Crustal structure surrounding the SAF exhibits significant along-strike variation, in intriguing correlation with the spatial pattern of upper crustal seismicity and deep NVT. Where the fault is transitional-to-creeping and characterized by microseismicity in the brittle crust, and where NVT is of lesser magnitude or absent, an overly conductive crust connects with the HCZ (Figs. 11, 12a). In turn, where the fault is transitional-to-locked, where only minor microseismic activity is observed in the upper crust, and where the majority of NVT episodes is localized at depths corresponding to the HCZ, the crust is above-average resistive between the SAF and the HCZ (Figs. 11, 12a).

As outlined previously, the crustal conductive zone imaged near the SAFOD has been suggested to represent a channel for deeply rooted fluids into the seismogenic SAF (Becken et al. 2008). The regional-scale MT data suggest that this crustal conductive zone connects directly with the HCZ at upper mantle depth; it is offset from the SAF surface trace to the southwest. This implies that the HCZ may correspond to the source region of mantle-derived fluids, which find pathways through crustal levels near the SAFOD (Becken et al. 2008, 2011) and which are responsible for the elevated mantle-derived gas concentration and fluid pressures east of the fault. In turn, and if fluids are responsible for the HCZ, these fluids appear to be trapped at greater depths farther southeast along the SAF, where such crustal pathways are absent, where the fault transitions to mechanical lock, and where NVT is observed.

3.3 Hydrated Mantle Wedge as the Fluid Source?

If fluids are responsible for the HCZ, what is the source of these fluids? In subduction zones, the subducting slab is an obvious source, either by direct dewatering in the early subduction stage, or by hydration-dehydration reactions with increasing slab depth and increasing temperatures and pressures (e.g., Wannamaker et al. 2010). Fluids released from the slab may percolate into the overlying mantle wedge, and go farther into the lower crust, and account for the high-conductivity anomalies there. In addition, aqueous fluids may support the formation of partial melts, which are for instance believed to persist beneath the Altiplano Plateau and which are responsible for a huge high-conductivity anomaly observed with MT (e.g., Schilling et al. 1997).

In central California, no such obvious fluid source exists, because subduction terminated $\sim$20 Ma ago. However, some authors have suggested that dehydration of a serpentinized relic mantle wedge, formed during subduction along coastal California in a way analogous to modern subduction systems, may still release fluids by ongoing dehydration reactions (Fig. 13).

Geodynamic and thermo-mechanical models of the ceased Farallon subduction include microplate capture, slab breakoff, and the formation of a slab window beneath the overriding North American plate (e.g., Nicholson et al. 1994; Wilson et al. 2005). In settings

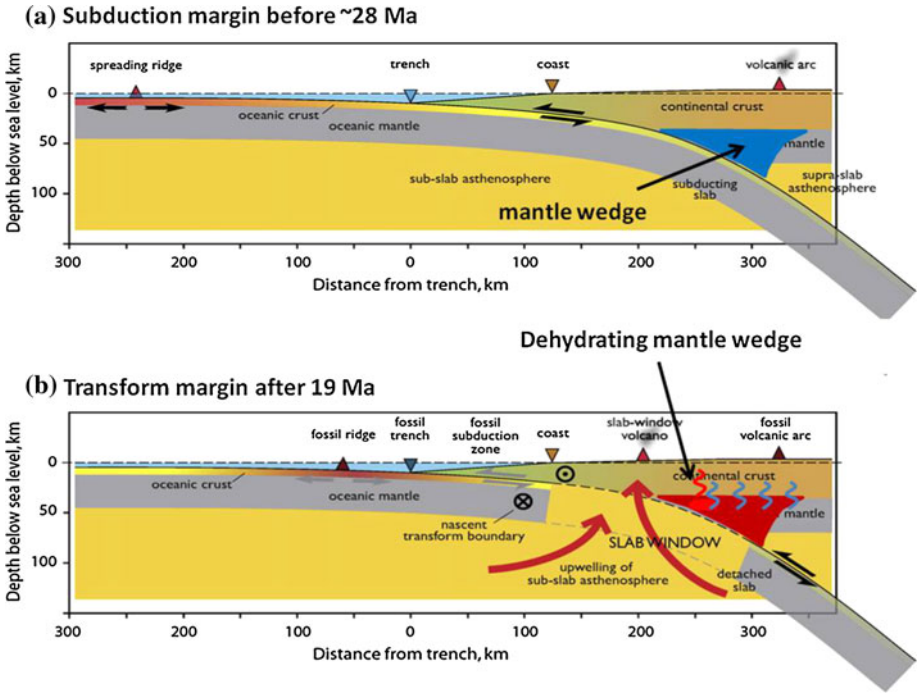

Fig. 13 Schematics of the evolution of the San Andreas transform margin, including capture of the remnant Monterey microplate, formation of a slab window and initiation of the transform margin near the slab tear, more than ~19 Ma ago. A serpentinized mantle wedge may have formed during the subduction history, and dehydration of this wedge may be an ongoing process (Fulton and Saffer 2009). Figure modified after McCrory et al. (2009)

where the oceanic ridge is near the trench (Fig. 13a), the buoyancy of the relatively young and hot downgoing slab material compensates for slab pull. This causes slow spreading and strong coupling between the overriding and downgoing plates. As a result, when slab-pull forces exceed the strength of the subducting plate, the downgoing slab tears and becomes accommodated in the mantle, and the two originally spreading plates become effectively one (McCrory et al. 2009). Such a breakoff scenario is considered for the ceased subduction and capture of the Monterey microplate in central California. When the slab tore beneath the overriding North American plate, the previously subducting Monterey microplate became attached to the Pacific plate. The asthenosphere that filled the forming slab window supplied a shallow heat source in direct contact with the overlying crust (Fig. 13b).

Based on this geodynamic scenario, Kirby et al. (2002) combined a detailed thermal model with a kinetic reaction model of serpentinite formation and dehydration to illustrate that the temperature increase following the migration of the Mendocino Triple Junction could drive continued prograde dehydration of serpentinized mantle for tens of millions of years, resulting in a large and sustained flux of water into the overlying crust. Numerical modeling and petrological constraints suggest that less than 10% of the mantle wedge was molten after the heat pulse following the Mendocine triple junction (MTJ) passage (Schmitt et al. 2006). In turn, more than 90% of the hydrated mantle wedge material would remain in place following MTJ passage where it would gradually dehydrate (Kirby et al. 2002).

Fulton and Saffer (2009) expanded this idea and demonstrated that dehydration of a persistent mantle wedge could account for the fluid overpressure (Fig. 7c) and the mantle-derived He signal observed near and within the SAFOD. Their calculations are based on dehydration of a volume of serpentinized mantle wedge corresponding to that of the modern mantle wedge beneath Cascadia sustained since the initiation of the SAF system, and on coupled heat and fluid flow modeling through a permeable upper crust with prescribed permeability. They further argue that fluid flux from a mantle wedge fluid source could generate isolated high fluid pressure pockets within an impermeable fault zone that acts as a barrier for fluid flow.

Similar conditions have been proposed for the modern Philippine Sea Plate subduction system in southeastern Japan. A compilation of $^{3}He/^{4}He$ ratios for southeastern Japan revealed systematic variations in the mantle-derived concentration in close association with geophysical evidence of a serpentinized fore-arc mantle wedge (Umeda et al. 2007). It was proposed that high $^{3}He/^{4}He$ ratios occur in regions where aqueous fluids derived from the subducting slab carry mantle-derived gas generated by a serpentinized mantle wedge. In turn, water is consumed in hydration reactions within a non-serpentinized mantle wedge, and the flux of fluids (and mantle-derived gas) is correspondingly low. Umeda et al. (2007) found that the occurrence of low-frequency earthquakes, believed to be caused by fluid migration from the slab into the lower crust, is spatially associated with elevated mantle-derived gas concentrations at the surface.

These considerations suggest that the HCZ imaged with MT at the SAF could originate from a dehydrating mantle wedge, in contrast to the situation in Japan where the source of fluids is more likely to be the subducting slab. The MT models in central California are consistent with the modeling scenario of Fulton and Saffer (2009) in suggesting permeable pathways through the crust into the creeping fault system. However, the geometrical interrelation between the resistivity model and the model of Fulton and Saffer is inconsistent. The MT model images a fluid source 20-40 km west of the SAF. The MT models further suggest that crustal pathways near SAFOD have an oblique, westward dipping geometry, running from the eastern fault block in the upper crust across the mid-crustal SAF to lower crustal and upper mantle levels beneath and west of the SAF. Fulton and Saffer (2009), on the other hand, placed the mantle wedge eastward of the SAF, based on observations that significant mantle-derived He was only found on the eastern fault block. Kirby et al. (2002) suggested that the mantle wedge should be at a distance of 60–250 km from the former trench, depending on variations of original slab dip. This distance range would agree with the model assumptions of Fulton and Saffer (2009), who place the wedge east of the present SAF, but also with the position of the HCZ west of the fault trace.

Fulton and Saffer (2009) also suggested that upper crustal fluid flow is controlled by NE-dipping faults and fractures within the country rock, with the ability to focus fluid flow into the brittle SAF. They argued that NE-dipping faults could be critically stressed and may thus act as the most permeable pathways for fluid flow (Townend and Zoback 2000). However, thrust faults in the Parkfield region penetrating into Franciscan rocks to mid-crustal levels or deeper, such as the Coalinga thrust and the San Joaquin thrust, exhibit a SW dipping geometry, whereas back-thrusts at the base of the Great Valley sequence, such as the Waltham Canyon thrust, exhibit dip to the NE (cf. Guzofski et al. 2007, Fig. 5). From earthquake data, Carena (2006) identified an active fault just east of the SAF near Parkfield that abuts the SAF near the bottom of the seismogenic crust ($\sim$15 km) (dashed line T in Fig. 8a). Furthermore, seismic waveform inversion across the SAF at SAFOD inferred a SW dipping reflector segment at lower crustal depth west of the SAF (element H in Fig. 8a, cf. Bleibinhaus et al. 2007), which could represent the lower crustal extension

of the thrust described by Carena (2006). Hence, there are strong indications for the existence of SW dipping faults, which could provide open pathways for fluid flow. This would be consistent with the MT observations which suggest a deep fluid source (mantle wedge) located west of the SAF, being linked across the seismogenic SAF and into the eastern fault block.

3.4 Relation with the Slab Window Geometry

In the previous sections, we argued that the HCZ corresponds to a ductile deformation zone and that fluids within the HCZ may be sourced in a dehydrating mantle wedge. If so, the position would provide constraints for the geometrical setting of a slab window model.

The slab window model implies that a proto-SAF was initiated near the slab tear zone, when the slab remnant was captured by the Pacific plate. Microplate capture induced transform motion into the overriding continental North American block and was facilitated by a thermal pulse of upwelling astenospheric material (Fig. 13). Geological evidence (e.g., Wilson et al. 2005), in agreement with thermo-mechanical and kinematic modeling (Nicholson et al. 1994), shows that the main strand of the brittle fault system "jumped" inland in several discrete steps into the current position of the SAF. These jumps were associated with inland diffusion of the ductile roots of the deformation system, probably triggered by lower crustal and upper mantle temperature diffusion, or controlled by integrated lithospheric strength variations (Popov 2009). This means that the ductile roots of the fault system were positioned between the ductile initiation zone of the SAF along the edge of the captured slab and its present position. This position could correspond to the source region of NVT sub-vertically below the seismically defined crustal portion of the fault, which is offset from the coast to the west.

The position of the slab tear is respect to the spreading center is still debated. Wilson et al. (2005) located the Monterey slab tear near the present coastline based on seismic imaging of the fossil plate fragment beneath the continental margin (Tréhu 1991) and on the distribution of forearc volcanism. Theoretical studies of slab tears typically assume a much deeper location for a detachment between 50 and 100 km depth where dehydration embrittlement of the slab is thought to occur. McCrory et al. (2009) propose that the tear can occur at much shallower depths of about 25 km, up-dip of a 450°C thermal threshold that marks the BD transition for quartzo-feldspathic-rich rocks in the accretionary prism. In either case, the ductile roots of the SAF system would be located inland of the breakoff-region. If the HCZ images the ductile deformation zone, then this would place the slab tear to the west of the HCZ, in agreement with models of Wilson et al. (2005), McCrory et al. (2009) and Popov (2009).

The slab geometry sketched in Fig. 13 implies that the mantle wedge developed further inland, i.e., east of the breakoff zone, and that this region does not coincide with the HCZ. However, it must be taken into account that the present-day geometry is integrating tectonic processes over geological times, including hundreds of kilometers of transform motion along the continental margin. This means that the present day location of the HCZ region is the result of tectonic processes and not an image of the initial conditions of the transform margin.

Remnants of the Monterey microplate exist offshore central California. Magnetic anomaly maps of fossil spreading centers (Fig. 14, after Nicholson et al. 1994) and documented phases of volcanism (Wilson et al. 2005) indicate that spreading and subduction of individual fragments of the Monterey Microplate ceased between 20 and 16 Ma, from south to north. It is important to note that subduction of the segmented ridge system has

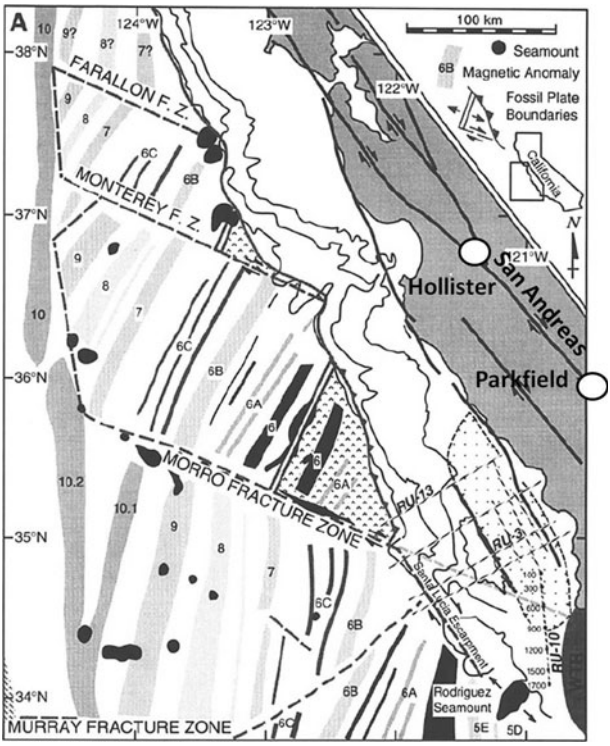

Fig. 14 Magnetic anomaly map showing the offshore extent of the remnant Monterey microplate in central California (Figure from Nicholson et al. 1994)

been characterized by episodic ridge deaths interspersed with intervals of fracture zone subduction (McCrory et al. 2009) and is an ongoing process in the Cascades.

Therefore, slab tear and mantle wedge formation may have occurred at variable distances from the coast and at different times, and separately for individual slab fragments. Subsequent reorganization of the continental margin by transform motion along the evolving SAF may have further complicated this geometrical relationships. Seismological mantle tomography (Schmandt and Humphreys 2010) reveals an actively subducting slab in the mantle beneath the Cascades as an elongated, trench-parallel high-velocity perturbation. In contrast, the velocity structure beneath the Californian Coast Ranges is more heterogeneous in the upper mantle (the model from Schmandt and Humphreys (2010) has been presented for >90 km depth), indicating that the slab window is not a continuous structure along coastal California and that its evolution was variable along-strike.

Note finally that the inland extrapolation of the Farallon and Monterey Fracture Zones abut the SAF approximately at Hollister and Parkfield, respectively (Fig. 14). The Monterey Fracture zones separate two fragments of the microplate, and the fossil spreading ridges are displaced along this fracture zone. As outlined before, it is unclear how far the Monterey microplate and thus the Fracture Zones extend beneath the continental margin, but it is possible that the geometry of the slab tear depends on the distance to the individual ridges and thus discontinues across the Fracture zone. This would add another complication to the geometrical setting beneath the continental edge.

4 Comparison with Other Major Fault Zones in the Earth's Crust

4.1 Niigata-Kobe Tectonic Zone (NKTZ), Japan

The NKTZ in central Japan is a 50–100 km wide and 500 km long deformation belt with high strain rates, historical and recent major earthquakes and a concentration of major fault zones. Among the different kinematic models that have been proposed for the NKTZ and that fit the observed GPS velocity vectors, a model containing a water-weakened lower crust and uppermost mantle is considered most plausible (e.g., Iio et al. 2004). A weak zone in the lower crust allows for concentration of viscous deformation within and influences the deformation regime in the upper crust. Upper crustal deformation is distributed over a number of strike-slip faults and to some extent accommodated by inelastic crustal deformation (Ohzono et al. 2011).

The NKTZ is characterized by significant along-strike heterogeneities in the crust and upper mantle, both in terms of geophysical parameters as well as in its mechanical behavior and magmatic activity. Heterogeneities within the NKTZ are believed to result from the complex interaction of the subducting Philippine and Pacific plates beneath Japan (Iio et al. 2004; Nakajima and Hasegawa 2007), the partial hydration of mantle wedges, local mantle convection geometries, and the shielding effect of the Philippine Plate lithosphere (Iio et al. 2004). Despite of these complications, lower crustal weakening is generally believed to originate from dehydration of the subducting plates, as has been observed elsewhere in subduction regimes (e.g., Wannamaker et al. 2010).

These conceptual models for the NKTZ system are largely based on the observation of pronounced electrical conductivity anomalies in the lower crust (e.g., Ogawa and Honkura 2004) and from the distribution of high $^{3}He/^{4}He$ isotope ratios (e.g., Umeda et al. 2007). Detailed 3D seismic traveltime tomography confirmed these models but also revealed a complicated, three-dimensional pattern of low- and high-velocity anomalies in the crust and upper mantle (Nakajima and Hasegawa 2007).

A number of MT studies concentrated on the Itoigawa-Shizuoka Tectonic line (ISTL) and the adjacent Atotsugawa fault system in the central part of the NKTZ (see Fig. 15). The ITSL is a major tectonic boundary which intersects the NKTZ obliquely and divides Japan tectonically into northeastern and southwestern Japan. This boundary poses a high risk of major earthquakes. MT resistivity imaging across the ISTL (profile label 1 in green circle) resolved prominent high-conductivity zones in the lower crust (labels C2m and C3m in Fig. 15d), possibly extending into the uppermost mantle, which were explained with partial melts (Ogawa et al. 2002) and aqueous fluids (Ogawa and Honkura 2004). The lower crustal conductor C2m beneath and west of the ITSL shows a clear depth to the top, corresponding to the cut-off depth of seismicity. This appears consistent with fluids stalled below the BD transition zone (cf. Jiracek et al. 2007), possibly at high pressures. Ogawa and Honkura (2004) proposed that fluid migration from this lower crustal conductive zone into more resistive upper crustal formations may trigger earthquakes. Two additional, shorter profiles across the ITSL (to the north and south, respectively) revealed along-strike-variations of the deep conductive zone, which suggests a laterally localized fluid distribution (Ogawa et al. 2002), or, alternatively, an oblique strike of conductivity anomalies with respect to the ITSL.

The MT data across the ITSL demonstrate a correlation between the extent of conductive zones in the lower crust and zones of strain accumulation inferred from kinematic contraction models based on GPS velocity estimates (Ohzono et al. 2011). These observations provide evidence for mechanical models assuming a weakened lower crust beneath

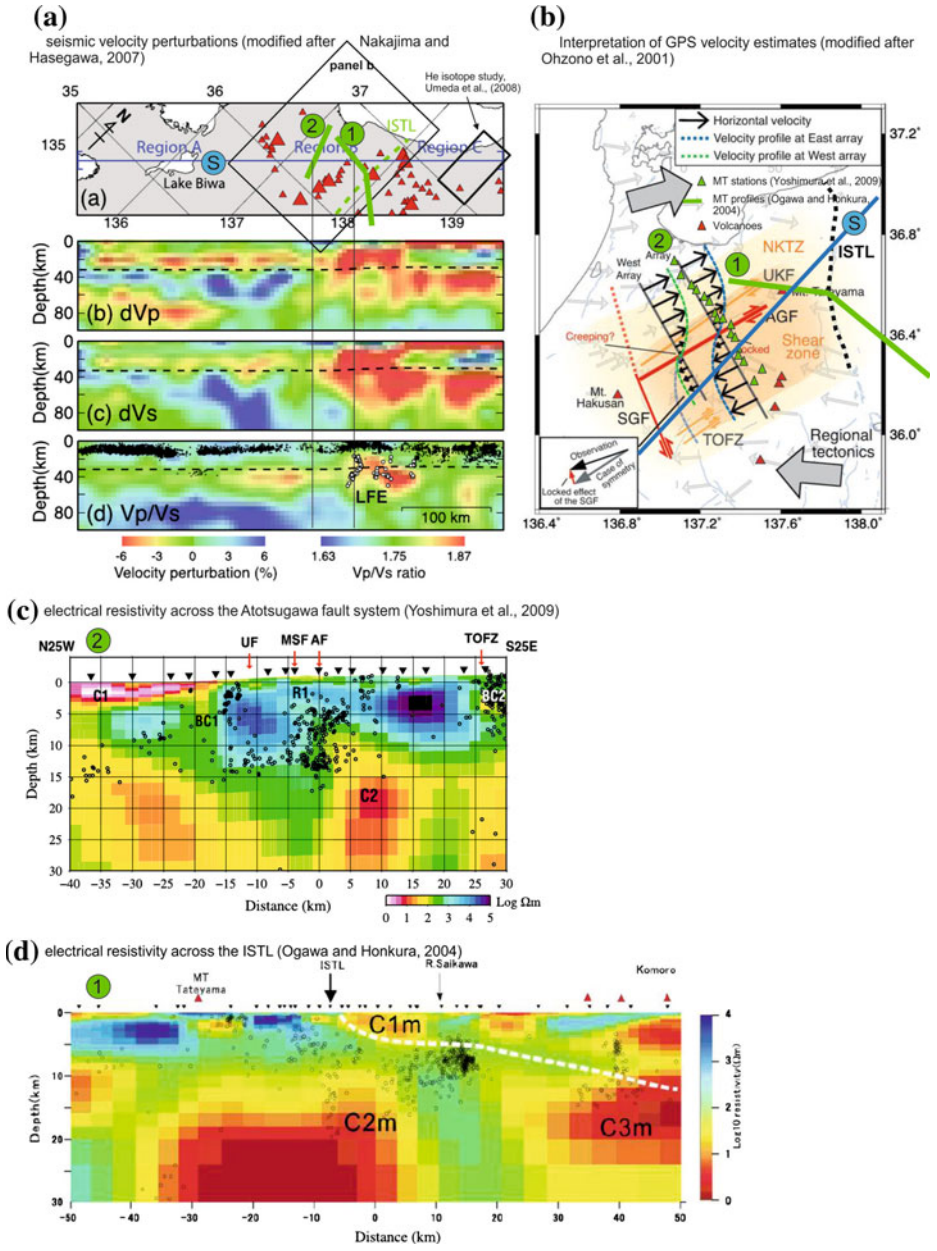

Fig. 15 Geophysical studies of the Niigata-Kobe Tectonic zone (*NKTZ*) in central Japan. **a** Location map and seismic velocity anomalies along the NKTZ (profile S, *blue line*) from Nakajima and Hasegawa (2007). **b** GPS velocity field. Changes along the Atotsugawa fault system indicate fault creep in the southwest (Ohzono et al. 2011). **c** MT resistivity structure at profile 2 (labels in *green circles*) across the Atotsugawa fault system (Yoshimura et al. 2009) and **d** at profile 1 across the Itoigawa-Shizuoka Tectonic line (*ISTL*) (Ogawa and Honkura 2004). Seismicity is superimposed. Location of MT profiles (*green*) and velocity section (*blue*) is indicated in **a** and **b**. See text for discussion

the NKTZ to explain the origin of the concentrated deformation zone in Japan (Iio et al. 2004). Furthermore, the resistivity structure strongly suggests that fluids influence the distribution of seismicity.

The Atotsugawa fault system fault system is part of the NKTZ and consists of three active strike-slip faults (UF, MSF and AF in Fig. 15c). Recent GPS velocity field estimations suggest that strain is heterogeneously distributed along the Atotsugawa fault system. The study of Ohzono et al. (2011) proposed aseismic surface creep toward a western branch of the fault as opposed to mechanical locking in the eastern part, closer to where the fault system meets the ITSL in the northeast.The main features of an MT profile (profile label 2 in green circle) across the Atotsugawa fault system presented by Yoshimura et al. (2009) are (1) a resistive zone (label R1 in Fig. 15c) with variable thickness in the upper crust, corresponding laterally to the extent of the NKTZ and (2) a pronounced high-conductivity zone (C2) in the lower crust intruding into the shallower resistor adjacent to the seismically defined deeper extension of the Atotsugawa fault (AF in Fig. 15c). Note that the spatial relationship between profiles 1 and 2 suggests that the conductive zones in the lower crust imaged along these profiles are connected. The observed high conductivities correlate spatially with a seismic low-velocity region (Fig. 15a). As for profile 2 an intrusion of fluids derived from the conductor C2 into the shallower resistor R1 is considered to influence the distribution of earthquakes, which are located within the resistor or close to the near-vertical boundary between the resistive and the conductive region.

Enhanced seismicity at shallow crustal levels along the Atotsugawa fault system is located beneath the Atotsugawa fault itself and at the boundaries of the upper crustal resistive zone where it is laterally sandwiched between more conductive formations beyond the NKTZ. Yoshimura et al. (2009) further pointed out that lateral variability of the crustal resistor correlates with variations in the strain rate observed at surface. They concluded that the high conductivity in the lower crust is caused by fluids, which results in lower crustal weakening and strain concentration controlling crustal deformation. Earthquakes may originate where fluids intrude in the resistive formations.

Yoshimura et al. (2009) extended previous MT studies of Goto et al. (2005), who measured another profile across the Atotsugawa fault system, where it exhibits creep. Although only few sites were measured, Goto et al. (2005) describe along-strike variations of upper crustal features along the fault. They found that a resistive zone appears uninterrupted across the fault where the fault appears to be locked at upper crustal levels. A resistive-conductive contrast coincides with the vertical downward extension of the creeping Atotsugawa fault. The authors suggested that the resistivity structure across the locked Atotsugawa fault is similar to resistivity images from the locked SAF at Carrizo Plain (Mackie et al. 1997), whereas the creeping Atotsugawa fault compares well with the creeping SAF, e.g., at Hollister (e.g., Bedrosian et al. 2004). However, the lacking spatial resolution of the data presented by Goto et al. (2005) hinders a more detailed comparison between the Atotsugawa fault and the SAF.

Expanded MT studies across the Atotsugawa fault system, including network MT measurements (Mogami et al. 2010) and joint inversion of broadband and Network MT data (Usui et al. 2010), were presented at the Giza, Egypt, induction workshop in 2010. These studies could improve the resolution of the two-dimensional resistivity structure at greater depth. Joint inversion of broadband and Network MT data confirmed the existence of a conducive zone in the lower crust and suggested that the conductive zones are localized beneath the active shear zones (Usui et al. 2010), in contrast to an uninterrupted lower crustal low compressional wave velocity anomaly. Possible explanations for the discrepancy between MT and seismic tomography results include variability in fluid

Fig. 16 **a** Tectonic map of Anatolia and adjacent areas. *Purple* profiles indicate locations of teleseismic cross-sections. *Black boxes* depict areas studied with MT and discussed in the text. **b** south–north and **c** west–east oriented profiles across Anatolia. *Left panels* show seismic velocity perturbations determined for the mantle (Biryol et al. 2011). *Right panels* show MT resistivity sections (Tank et al. 2005, Türkoglu et al. 2008). Approximate extent of the resistivity model in **b** is indicated on the velocity model. In **c** *black lines* depict intersections of the velocity model with the resistivity model. Seismicity (*black dots*) is superimposed on the resistivity sections. See text for discussion ▶

interconnectivity, to which electrical resistivity responds more sensitively than the seismic p-velocity (Usui et al. 2010).

A confined source region of tremor, composed of a sequence of low-frequency earthquakes (labeled LFE in Fig. 15a), appears in north–south direction and in the depth range of 20–40 km. At this depth, the LFEs are clearly below the seismogenic crust, but cannot be directly related to the subducting slab. These LFEs originate from around low-velocity anomalies imaged with traveltime tomography. The spatial relation between electrical conductivity structures and low-frequency earthquakes was not investigated in any detail. However, from the Fig. 15, the LFEs appear spatially associated with the edges of the conductive zone labeled C2 in Fig. 15c and C2m in Fig. 15d. Note that the LFEs were observed at the presumed locked segment of the Atotsugawa fault system and close to the transition where fault creep was proposed based and GPS velocity fields. Further investigations would be necessary to examine a possible relation between fault creep, fluid-induced high-conductivity zones and the distribution of LFEs, similar to the investigations of the Parkfield–Cholame segment of the SAF zone in California.

4.2 North Anatolian Fault Zone

The North Anatolian Fault (NAF) is a right-lateral strike-slip fault crossing the entire length of Northern Turkey, roughly in parallel with the southern coast of the Black Sea (Fig. 16a). The NAF and the SAF can appear as twins due to their similar length and geometry. While they share important similarities, there are also important differences between the two fault systems.

The NAF was initiated after the closure of the Tethys ocean. Because the continental crust was too buoyant to be subducted, subduction of the Tethys oceanic crust ceased and was followed by continental collision. This change in the style of deformation and convergence was accommodated by the extrusion of the Anatolian block to the west and crustal thickening to the east. The fate of the subducted plate beneath Eurasia is not entirely clear. One class of geodynamic models suggests that the oceanic slab tore, followed by astenospheric upwelling and the uplift of the Anatolian plateau in response to elevated upper mantle temperatures (e.g., Keskin 2003; Biryol et al. 2011). In comparison, the SAF was initiated when subduction of the Farallon plate ceased following slab breakoff and the capture of the western continental margin by the underriding remnant of the Pacific plate (e.g., McCrory et al. 2009). In California, subduction ceased because the spreading center collided with the continent, whereas subduction in Anatolia ceased because two continents collided. This implies that the thermodynamical regimes following the initiation of the two shear zones developed differently. In particular, heat flow in Turkey is spatially heterogeneous, with regions of elevated heat flow of up to 100–200 mW/m^2 in western (Ilkisik 1995), central, and eastern Anatolia, and with intervening regions of lesser heat flow (Basel et al. 2010).

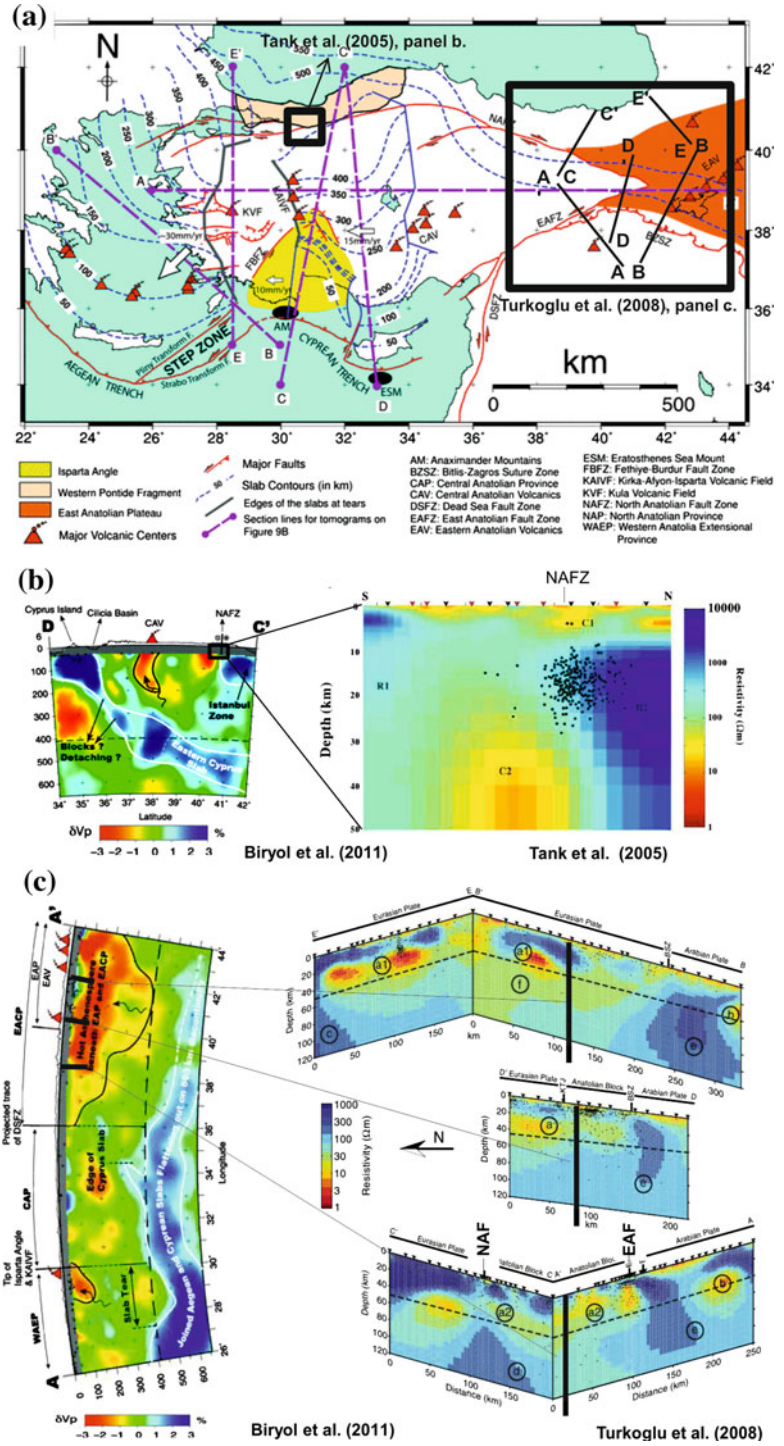
(a)
Tank et al. (2005), panel b.
Turkoglu et al. (2008), panel c.
N
km
0
500
STEP ZONE
AEGEAN TRENCH
CYPREAN TRENCH
KVF
KAIVF
FBFZ
DSFZ
CAV
EAV
EAFZ
BZSZ
NAF
AM
ESM
Isparta Angle
Western Pontide Fragment
East Anatolian Plateau
Major Volcanic Centers
Major Faults
Slab Contours (in km)
Edges of the slabs at tears
Section lines for tomograms on Figure 9B
AM: Anaximander Mountains
BZSZ: Bitlis-Zagros Suture Zone
CAP: Central Anatolian Province
CAV: Central Anatolian Volcanics
DSFZ: Dead Sea Fault Zone
EAFZ: East Anatolian Fault Zone
EAV: Eastern Anatolian Volcanics
ESM: Eratosthenes Sea Mount
FBFZ: Fethiye-Burdur Fault Zone
KAIVF: Kirka-Afyon-Isparta Volcanic Field
KVF: Kula Volcanic Field
NAFZ: North Anatolian Fault Zone
NAP: North Anatolian Province
WAEP: Western Anatolia Extensional Province
(b)
Cyprus Island
Cilicia Basin
CAV
NAFZ
Istanbul Zone
Blocks ? Detaching ?
Eastern Cyprus Slab
Latitude
δVp
%
Biryol et al. (2011)
NAFZ
Depth (km)
Resistivity (Ωm)
Tank et al. (2005)
(c)
Projected trace of DSFZ
EAP
EAV
EACP
CAP
WAEP
Tip of Isparta Angle & KAIVF
Edge of Cyprus Slab
Slab Tear
Longitude
Biryol et al. (2011)
Eurasian Plate
Arabian Plate
Anatolian Block
NAF
EAF
Distance (km)
Turkoglu et al. (2008)

Fault creep is also observed along small portions of the NAF. However, these sections are still capable of producing major earthquakes, because only 30–50% of the yearly slip is accommodated by surface creep (Karabacak et al. 2011). Recent creep observations in central California have revealed that $\sim$70% of geodetic slip rates are accommodated by fault creep (25 mm/a surface creep as opposed to 35 mm/a far field slip rates; cf. Titus et al. 2005; Toke et al. 2011).

There are a number of MT studies of the NAF. Türkoglu et al. (2008) presented resistivity models from the Karliova Triple Junction area in eastern Turkey. Long-period MT observations along several profiles were measured in an area covering approximately 300 km $\times$ 400 km in the east-west and north-south directions. The profiles were arranged across the Anatolian Block which is wrenched between the East Anatolian fault (EAF) and NAF systems and across the Eastern Anatolian Plateau in the east of the Karliova Triple Junction (cf. Fig. 16a). Low resistivities ($10 - 20\,\Omega$m) were encountered in the lower crust beneath the Anatolian block. Beneath the Eastern Anatolian Plateau, pockets of very low resistivities ($\sim 3\,\Omega$m) were detected in the lower crust, underlain by anomalously low resistivities ($30\,\Omega$m) in the upper mantle, as opposed to resistivities of $300\,\Omega$m in the upper mantle beneath the Arabian Plate in the south and the Anatolian Block in the west (Fig. 16c, right panel). Türkoglu et al. (2008) explained the low resistivities in the lower crust and upper mantle with the presence of partial melts (3–10% in the very low resistive pockets beneath the Anatolian Plateau and 1% in the anomalously conducting upper mantle) and, more generally, aqueous fluids and/or partial melts in the lower crust beneath the Anatolian Block. The low resistivities appear overall coincident with low P-velocity and strong S-wave attenuation.

These results suggest that the low-resistive zones correspond to mechanically weak zones, which may permit lateral flow in the lower crust and upper mantle and may perhaps also indicate a decoupling of the upper and lower lithosphere (Türkoglu et al. 2008). A recently presented teleseismic P-wave tomography of the Anatolian region showed extended low-velocity anomalies beneath the Eastern Anatolian Plateau rooted deeply in the upper mantle (Biryol et al. 2011) (Fig. 16c, left panel). These results strongly confirm an interpretation that assumes widespread upwelling of hot astenosphere beneath the Eastern Anatolian Plateau.

The resistivity structure also imaged the crustal structure surrounding the EAF and NAF zones. In the model of Türkoglu et al. (2008) in Fig. 16c (right panel), the EAF is associated with a pronounced, near-vertical conductive zone, which extends from $\sim$10 to 15 km depth to the base of the crust at $\sim$50 km. The high conductivities are bounded above and laterally to the south by a resistive block. The resistor appears rooted in the mantle beneath the Arabian Plate, but extends at shallower levels laterally uninterrupted across the Bitlis-Poturge Suture zone and the EAF. There is no obvious correlation between resistivity structure or resistive–conductive boundaries and the distribution of seismicity.

In contrast, crustal resistivities beneath the NAF are modest. A 20–40 km wide conductive pocket was imaged in the lower crust beneath the Eurasian Plate, centered approximately 50 km to the north of the NAF. However, its relation to the NAF system is not clear.

Türkoglu et al. (2008) argue that it "is possible that (1) fluids are controlling the observed deformation through weakening the lithosphere, or (2) the deformation produces zones of enhanced fluid content through maintaining a network of interconnected cracks". For Anatolia, they propose that fluids causing the anomalous conductivity of the astenosphere beneath the Eastern Anatolian plateau could also cause rheological weakening. The crustal conductive zone beneath the EAF zone could correspond to a strain-generated fracture network occupied by fluids.

The complicated tectonic setting surrounding the Karliova Triple Junction may not be representative for the entire strike-slip fault system of Anatolia. Teleseismic tomography results from a cross-section which is in its central part approximately coincident with the MT profiles AA' and CC' shown by Türkoglu et al. (2008) show low seismic velocity in the mantle and no correlation with either of the Anatolian block boundaries (Biryol et al. 2011). In stark contrast, mantle velocity across the western parts of the NAF indicates a first-order velocity contrast vertically beneath the fault zone which penetrates to depths of 100–150 km (Fig. 16b, left panel). Here, the faster region north of the NAF is associated with old and colder lithosphere of the Istanbul zone (Biryol et al. 2011).

Several crustal MT profiles were measured across the NAF in western Anatolia. These profiles are located close to the Izmit (Mw = 7.4) and the Düzce (Mw = 7.2) earthquakes, which occurred in 1999. In Fig. 16b (right panel), we depict as an example the resistivity structure described by Tank et al. (2005). Here, the surface trace of the NAF separates into two branches. The northern branch of the NAF is associated with seismicity which is localized near a prominent near-vertical resistivity contrast at depth (Fig. 16b). The southern branch is seismically less active and associated with a less pronounced resistivity increase toward the south. Intervening between these two branches, resistivity values are moderate at upper crustal levels. The most prominent feature of the model is a conductive zone at lower crustal depth, which extends laterally between the northern and the southern branches of the NAF. This conductive zone has been explained with the presence of partial melts, and with fluids released into shallower levels. In analogy to the NKTZ, the lower crust beneath the NAF is presumably weak, which can result in the concentration of strain, and in the generation of major earthquakes, possibly triggered by fluid released into the earthquake source region.

5 Summary and Conclusions

Fluids play a key role in the mechanics and dynamics of faulting. MT is powerful in delineating high-conductivity zones, and aqueous fluids residing in interconnected porosity networks often provide a plausible explanation. Therefore, MT can help to constrain tectonic processes by illuminating the distribution of fluids and fluid pathways. In this paper, we examine MT results from the SAF zone with other geophysical and geochemical observations, and geodynamic models to address the source regions of fluids and mechanisms that may have generated pathways for fluids. In doing so, a scenario evolved that fits into modern geodynamic models and that can help to explain variations in the seismic behavior of the fault. The regional-scale MT studies focused on the Parkfield–Cholame segment of the SAF in central California, where the fault is transitional from mechanical lock to aseismic creep. Therefore, it remains an open question whether or not fluid-based scenarios presented here are representative for the entire fault (or larger portions of it).

It is now well established from many examples worldwide that interconnected fluid networks have a weakening effect on the rheology of rocks. The models and mechanisms proposed from the MT data suggest an occurrence and supply of fluids and the formation of fluid networks at all depth levels, from the upper crust into the upper mantle, with apparently important implications for the mechanical state of the SAF.

In the upper few kilometers of the fault, active deformation facilitates the formation of a FZC. A FZC has been observed at different positions along the creeping segment of the fault and its conductance depends on fault activity. Repeated cycles of healing and shearing could be responsible for the formation of broad (several hundreds of meters) fault

damage zones. Ritter et al. (2005) exemplified how the geometry and conductivity of a FZC in combination with seismicity can help to decipher architectural units and hydraulic characteristics of the fault zone. However, not all active shear zones are associated with FZCs. It is unlikely that the mechanical properties of the upper few kilometers determine the position and behavior of entire fault zone; therefore, a FZC is probably a feature that develops and is maintained in response to strain, but if well developed has the potential to determine the style of deformation and support surface creep.

Along the Parkfield–Cholame segment, regional-scale MT profiles identified a high-conductivity zone in the lower crust and upper mantle offset from the SAF surface trace toward the coast (Becken et al. 2011). The high conductivity could be caused by a dehydrating mantle wedge region (Kirby et al. 2002; Fulton and Saffer 2009). Fluids sourced in the mantle wedge find pathways into weak crustal zones coinciding spatially with exhumation paths of serpentinite (Kirby et al. 2002). These pathways appear as uninterrupted, sub-vertical conductive zones (Becken et al. 2008) which intersect the SAF at depth near the brittle-ductile transition zone and which feed a fluid reservoir in the eastern fault block (Unsworth and Bedrosian 2004a; Becken et al. 2008). This could explain SAFOD observations of fluid chemistry and hydrology (Zoback et al. 2006; Wiersberg and Erzinger 2007), including overpressured fluids in the eastern fault block (Johnson and McEvilly 1995; Zoback et al. 2010). Serpentinite or reaction products derived from serpentinite, such as talc (Moore and Rymer 2007), other weak minerals and high pressure fluids (Irwin and Barnes 1975; Rice 1992; Fulton and Saffer 2009), can all contribute to the weakness of the fault where it exhibits aseismic creep.

However, SAFOD observations do not strictly support the idea that high pressure fluids play an important role for fault creep, because in situ observations from the fault core, where it was drilled, provided no evidence for elevated fluid pressures. This suggests that where the SAF was intersected by the SAFOD borehole is not representative of the entire fault zone (Fulton and Saffer 2009) or that fault zone models involving high fluid pressures must be reconsidered.

Where the fault is locked, the crust is above-average resistive between the inferred mantle wedge region and the SAF (Becken et al. 2011). Here, outcrops of serpentinite are unknown which may suggest that serpentinite was not exhumed along the locked segment and that fluids are trapped near the mantle wedge source region. Ongoing dehydration and fluid trapping in this region could result in high fluid pressures and trigger brittle-like rock failure in nearby critically stressed domains. This agrees with the presence of near-lithostatic fluid pressures inferred for the source region of NVT near Cholame (Nadeau and Dolenc 2005; Thomas et al. 2009; Shelly 2010).

Magnetotelluric studies from other fault segments, such as Hollister or Carrizo Plain, are limited in their spatial extent and period range and cannot resolve lower crustal or upper mantle structure. If fluids of mantle origin play an important role for the creeping behavior of the fault, as inferred for the Parkfield region, we would expect that a deep fluid source and crustal pathways for fluids exist along all of the creeping segments of the SAF. In turn, fluids trapped below the (mid-)crust could be characteristic of the locked segment of the SAF, such as the Cholame region. To test this more systematically would require additional MT data.

Many active tectonic areas worldwide are associated with zones of high electrical conductivity in the lower crust and upper mantle. For the Niigata-Kobe tectonic zone in Japan, it was shown that a water-weakened lower crust results in concentrated deformation (Ogawa and Honkura 2004). Developing shear zones in the Marlborough region in New Zealand are spatially associated with weak zones in the lower crust originating from the

influx of fluids released from the subducting plate (Wannamaker et al. 2010). Lower crustal flow due to the weakening effect of fluids has also been proposed for the Eastern Anatolian Plateau (Türkoglu et al. 2008) and the Tibetan Plateau (e.g., Unsworth 2010). These observations suggest that fluids present in the roots of fault zones or collision zones have the potential to affect the deformation regime.

Jiracek et al. (2007), among others, argued that fluids below the seismogenic zone play an active role in the rupture process. The models discussed in this work include fluids breaching the BD transition zone, which is normally an obstacle for upward fluid flow. Fluid release into the upper crust can result in high fluid pressures and consequently in the generation of earthquakes. While this model is widely accepted, it remains unclear whether the presence or absence of fluids determines the strength of an entire fault segment and, ultimately, the distribution of fault creep and fault lock.

Acknowledgments We wish to express our sincere thanks to the Program Committee and LOC of the Giza workshop, who offered us a chance to prepare and deliver this review. We also thank the guest editors of the review volume, T. Korja and N. Palshin, for their guidance and patience, and two reviewers for their constructive comments.

References

Basel EDK, Satman A, Serpen U (2010) Predicted subsurface temperature distribution maps for Turkey. In: Proceedings world geothermal congress 2010, Bali, Indonesia, 25–29 April 2010

Becken M, Burkhardt H (2004) An ellipticity criterion in magnetotelluric tensor analysis. Geophys J Int 159:69–82

Becken M, Ritter O, Park SK, Bedrosian PA, Weckmann U, Weber M (2008) A deep crustal fluid channel into the San Andreas Fault system near Parkfield, California. Geophys J Int 173:718–732

Becken M, Ritter O, Bedrosian PA, Weckmann U (2011) Correlation between deep fluids, tremor and creep along the central San Andreas Fault. Nature 480(7375):87–90

Bedrosian PA, Unsworth MJ (2003) Magnetotelluric constraints on the nature of lower-crustal shear zones. AGU fall meeting abstracts, December 2003, p B8+

Bedrosian PA, Unsworth MJ, Egbert GD, Thurber CH (2004) Geophysical images of the creeping segment of the San Andreas Fault: implications for the role of crustal fluids in the earthquake process. Tectonophysics 385:137–156

Bennington N, Thurber C, Roecker S (2008) Threedimensional seismic attenuation structure around the SAFOD site, Parkfield, California. Bull Seismol Soc Am 98:2934–2947

Biryol CB, Beck SL, Zandt G, Ozacar AA (2011) Segmented African lithosphere beneath the Anatolian region inferred from teleseismic P-wave tomography. Geophys J Int 184:1037–1057

Bleibinhaus F, Hole JA, Ryberg T, Fuis GS (2007) Structure of the California coast ranges and San Andreas Fault at SAFOD from seismic waveform inversion and reflection imaging. J Geophys Res 112:B06315

Bürgmann R, Dresen G (2008) Rheology of the lower crust and upper mantle: evidence from rock mechanics, Geodesy, and Field Observations. Annu Rev Earth Planet Sci 36:531–567

Buske S, Gutjahr S, Rentsch S, Shapiro SA (2007) Application of Fresnel-volume-migration to the SAFOD2003 data set. In: EAGE 69th annual meeting and technical exhibition, extended abstracts

Byerlee J (1990) Friction, overpressure and fault normal compression. Geophys Res Lett 17:2109–2112

Caine JS, Evans JP, Evans CP, Foerster CP (1996) Fault zone architecture and permeability structure. Geology 24:1125–1128

Carena S (2006) 3-D geometry of active deformation east of the San Andreas Fault near Parkfield, California. AGU fall meeting abstracts, December 2006, p C178+

Chéry J, Zoback MD, Hickman S (2004) A mechanical model of the San Andreas Fault and SAFOD pilot hole stress measurements. Geophys Res Lett 31:L15S13

Connolly JAD, Podladchikov YY (2004) Fluid flow in compressive tectonic settings: implications for midcrustal seismic reflectors and downward fluid migration. J Geophys Res 109:B04201

Cox SF (2005) Coupling between deformation, fluid pressures, and fluid flow in ore-producing hydrothermal systems at depth in the crust. In: Hedenquist JW, Thompson JFH, Goldfarb RJ, Richards JP (eds) Economic geology 100th anniversary volume. Econ Geol, pp 39–76

Dickinson WR, Rosenberg LI, Greene HG, Graham SA, Clark JC, Weber GE, Kidder S, Gary Ernst W, Brabb EE (2005) Net dextral slip, Neogene San Gregorio, Hosgri fault zone, coastal California: geologic evidence and tectonic implications. Geological Society of America special paper 391, pp 1–43

Eberhart-Philips D, Stanley WD, Rodriguez BD, Lutter WJ (1995) Surface seismic and electrical methods to detect fluids related to faulting. J Geophys Res 100(B7):12919–12936

Field EH, Milner KR, and the 2007 Working Group on California Earthquake Probabilities (2008) Forecasting california's earthquakes; what can we expect in the next 30 years? Technical report, U.S. Geological Survey, Fact Sheet 2008-3027, p 4

Fulton PM, Saffer DM (2009) Potential role of mantle-derived fluids in weakening the San Andreas Fault. J Geophys Res 114:B07408

Fulton PM, Schmalzle G, Harris RN, Dixon T (2010) Reconciling patterns of interseismic strain accumulation with thermal observations across the Carrizo segment of the San Andreas Fault. Earth Planet Sci Lett 300:402–406

Goto T, Wada Y, Oshiman N, Sumitomo N (2005) Resistivity structure of a seismic gap along the Atotsugawa Fault, Japan. Phys Earth Planet Inter 148:55–72

Gueguen Y, Palciauskas V (1994) Introduction to the physics of rocks. Princeton University Press, Princeton

Gürer A, Bayrak M (2007) Relation between electrical resistivity and earthquake generation in the crust of West Anatolia, Turkey. Tectonophysics 445:49–65

Guzofski CA, Shaw JH, Lin G, Shearer PM (2007) Seismically active wedge structure beneath the Coalinga anticline, San Joaquin basin, California. J Geophys Res 112:B03S05

Hashin Z, Shtrikman S (1962) Electrical conductances of aqueous sodium chloride solutions from 0 to 800° and at pressures to 4000 bars. J Appl Phys 33:3125–3131

Hickman S, Zoback M, Ellsworth W (2004) Introduction to special section: preparing for the San Andreas Fault observatory at depth. Geophys Res Lett 31:L12S01

Hoffmann-Rothe A, Ritter O, Janssen C (2004) Correlation of electrical conductivity and structural damage at a major strike-slip fault in northern Chiley. J Geophys Res 109:B10101

Hole JA, Ryberg T, Sharma AK, Fuis SG (2004) Seismic velocity structure from a refraction–reflection survey across the San Andreas Fault at SAFOD. San Francisco, AGU fall meeting

Iio Y, Sagiya T, Kobayashi Y (2004) Origin of the concentrated deformation zone in the Japanese islands and stress accumulation process of intraplate earthquakes. Earth Planets Space 56:831–842

Ilkisik OM (1995) Regional heat flow in western Anatolia using silica temperature estimates from thermal springs. Tectonophysics 42:175–184

Irwin WP (1990) Geology and plate-tectonic development, chapter 3. The San Andreas Fault system in California. United States Geological Survey, professional paper 1515

Irwin WP, Barnes I (1975) Effect of geologic structure and metamorphic fluids on seismic behavior of the San Andreas Fault system in central and northern California. Geology 3:713–716

Jiracek GR, Gonzalez VM, Caldwell TG, Wannamaker PE, Kilb D (2007) Seismogenic, electrically conductive, and fluid zones at continental plate boundaries in New Zealand, Himalaya, and California, USA. In: Okaya D, Stern T, Davey F (eds) A continental plate boundary: tectonics at South Island, New Zealand, Geophysical Monogaph Series AGU, vol 175, pp 347–369

Johnson PA, McEvilly TV (1995) Parkfield seismicity: fluid-driven. J Geophys Res 100:12937–12950

Kappler KN, Morrison HF, Egbert GD (2010) Long-term monitoring of ULF electromagnetic fields at Parkfield, California. J Geophys Res 115:B04406

Karabacak V, Altunel E, Cakir Z (2011) Monitoring aseismic surface creep along the North Anatolian Fault (Turkey) using ground-based LIDAR. Earth Planet Sci Lett 304(1–2):64–70. ISSN:0012-821X; doi: 10.1016/j.epsl.2011.01.017.

Kennedy BM, Kharake YK, Evans WC, Ellwood A, DePaolo DJ, Thordsen J, Mariner RH (1997) Mantle fluids in the San Andreas Fault system, California. Science 278:1278–1281

Keskin M (2003) Magma generation by slab steepening and breakoff beneath a subduction-accretion complex: an alternative model for collision-related volcanism in Eastern Anatolia, Turkey. Geophys Res Lett 30:8046

Kharaka YK, Thordsen JJ, Evans WC, Kennedy BM (1999) Geochemistry and hydromechanical interactions of fluids associated with the San Andreas Fault system, California. In: Haneberg WC, Mosely PS, Moore JC, Goodwin LB (eds) Faults and subsurface fluid flow in the shallow crust, vol 113 of Geophysical monograph. American Geophysical Union, Washington, DC, pp 129–148

Kirby SH, Wang K, Brocher T (2002) A possible deep, long-term source for water in the Northern San Andreas Fault system: a ghost of Cascadia subduction past? Eos Trans AGU 83:Fall Meeting Supplement Abstract S22B-1038

Li YD, Malin PE (2008) San Andreas Fault damage at SAFOD viewed with fault-guided waves. Geophys Res Lett 35:L08304

Mackie RL, Livelybrooks DW, Madden TR, Larsen JC (1997) A magnetotelluric investigation of the San Andreas Fault at Carrizo Plain, California. Geophys Res Lett 24:1847–1850
Madden TR, LaTorraca GA, Park SK (1993) Electrical conductivity variations around Palmdale section of the San Andreas Fault zone. J Geophys Res 98:795–808
McCrory PA, Wilson DS, Stanley RG (2009) Continuing evolution of the Pacific-Juan de Fuca-North America slab window system—a trench-ridge-transform example from the Pacific Rim. Tectonophysics 464:30–42
McPhee DK, Jachens RC, Wentworth CM (2004) Crustal structure across the San Andreas Fault at the SAFOD site from potential field and geologic studies. Geophys Res Lett 31:L12S03
Mogami T, Yamaguchi S, Uyeshima M, Ogawa T, Usui Y, Murakami H, Tambo T, Toh H, Oshiman N, Yoshimura R, Koyama S, Mochizuki H (2010) Geoelectric structure around the Niigata Kobe Tectonic zone inferred from Network-MT survey. In: 20th international workshop on electromagnetic induction, Giza, Egypt
Moore DE, Rymer MJ (2007) Talc-bearing serpentinite and the creeping section of the San Andreas Fault. Nature 448:795–797
Nadeau RM, Dolenc D (2005) Nonvolcanic tremors deep beneath the San Andreas Fault. Science 21:389
Nakajima J, Hasegawa A (2007) Deep crustal structure along the niigata-kobe tectonic zone, Japan: its origin and segmentation. Earth Planets Space 59:e5–e8
Nicholson C, Sorlien CC, Atwater T, Crowell JC, Luyendyk BP (1994) Microplate capture, rotation of the western transverse ranges, and initiation of the San Andreas transform as a low-angle fault system. Geology 22:491–495
Obara K (2002) Nonvolcanic deep tremor associated with subduction in Southwest Japan. Science 31:1679–1681
Ogawa Y, Honkura Y (2004) Mid-crustal electrical conductors and their correlations to seismicity and deformation at Itoigawa-Shizuoka tectonic line, Central Japan. Earth Planets Space 56:1285–1291
Ogawa Y, Takakura S, Honkura Y (2002) Crustal deformation around the northern and central Itoigawa-Shizuoka tectonic line. Earth Planets Space 54:1059–1063
Ohzono M, Sagiya T, Hirahara K, Hashimoto M, Takeuchi A, Hoso Y, Wada Y, Onoue K, Ohya F, Doke R (2011) Strain accumulation process around the Atotsugawa fault system in the Niigata-Kobe Tectonic Zone, central Japan. Geophys J Int 184:977–990
Ozacar AA, Zandt G (2009) Crustal structure and seismic anisotropy near the San Andreas Fault at Parkfield, California. Geophys J Int 178:1098–1104
Page BM, Thompson GA, Coleman RG (1998) Late Cenozoic tectonics of the central and southern Coast Ranges of California. GSA Bull 110:846–876
Park SK, Larsen JC, Lee T-C (2007) Electrical resistivity changes not observed with the 28 September 2004 M6.0 Parkfield earthquake on the San Andreas Fault, California. J Geophys Res 112:B12305
Pili E, Kennedy BM, Conrad MS, Gratier JP (1998) Isotope constraints on the involvement of fluids in the San Andreas Fault. EOS Trans AGU 79:229–230
Popov AA (2009) Three-dimensional thermo-mechanical modeling of deformation at plate boundaries: case study San Andreas Fault system. PhD thesis, Potsdam University
Quist AS, Marshall AL (1968) Electrical conductances of aqueous sodium chloride solutions from 0 to 800° and at pressures to 4000 bars. J Phys Chem 72:684–703
Rice JR (1992) Fault stress states, pore pressure distributions, and the weakness of the San Andreas Fault. In: Evans B, Wong T-F (eds) Fault mechanics and transport properties of rocks. Academic, San Diego, CA, pp 475–503
Ritter O, Haak V, Rath V, Stein E, Stiller M (1999) Very high electrical conductivity beneath the Münchberg Gneiss area in Southern Germany: implications for horizontal transport along shear planes. Geophys J Int 139:161–170
Ritter O, Hoffmann-Rothe A, Bedrosian PA, Weckmann U, Haak V (2005) Electrical conductivity images of active and fossil fault zones. In: Bruhn D, Burlini L (eds) In high-strain zones: structure and physical properties, vol 245. Geological Society of London Special Publications, pp 165–186
Ryberg T, Fuis GS, Bauer K, Hole JA, Bleibinhaus F (2005) Upper-Crustal Reflectivity of the central California Coast Range Near the San Andreas Fault Observatory at Depth (SAFOD), USA. AGU Fall Meeting Abstracts, December 2005, p A441+
Ryberg T, Haberland C, Fuis GS, Ellsworth WL, Shelly DR (2010) Locating non-volcanic tremor along the San Andreas Fault using a multiple array source imaging technique. Geophys J Int 183:1485–1500
Sass JH, Williams CF, Lachenbruch AH, Galanis SP Jr, Grubb FV (1997) Thermal regime of the San Andreas Fault near Parkfield, California. J Geophys Res 102:27575–27585

Schilling FR, Partzsch GM, Brasse H, Schwarz G (1997) Partial melting below the magmatic arc in the central andes deduced from geoelectromagnetic field experiments and laboratory data. Phys Earth Planet Inter 103:17–32
Schmandt B, Humphreys E (2010) Complex subduction and small-scale convection revealed by body-wave tomography of the western united states upper mantle. Earth Planet Sci Lett 297:435–445
Schmitt AK, Romer R, Stimac J (2006) Geochemistry of volcanic rocks from the Geysers geothermal reservoir, Californian Coast Ranges. Lithos 87:80–103
Schmucker U (1970) Anomalies of geomagnetic variations in the Southwestern United States. University of California Press, Berkeley
Scholz CH (2002) The mechanics of earthquakes and faulting, 2nd edn. Cambridge University Press, Cambridge
Schwartz SY, Rokosky JM (2007) Slow slip events and seismic tremor at circum-pacific subduction zones. Rev Geophys 45:RG3004
Shelly DR (2010) Migrating tremors illuminate deformation beneath the seismogenic San Andreas Fault. Nature 463:648–652
Shelly DR, Beroza GC, Ide S, Nakamula S (2006) Low-frequency earthquakes in Shikoku, Japan and their relationship to episodic tremor and slip. Nature 442
Shelly DR, Ellsworth WL, Ryberg T, Haberland C, Fuis GS, Murphy J, Nadeau RM, Bürgmann R (2009) Precise location of San Andreas Fault tremors near Cholame, California using seismometer clusters: slip on the deep extension of the fault? Geophys Res Lett 36:L01303
Tank SB, Honkura Y, Ogawa Y, Matsushima M, Oshiman N, Tuncer MK, Celik C, Tolak E, Isikara AM (2005) Magnetotelluric imaging of the fault rupture area of the 1999 Izmit (Turkey) earthquake. Phys Earth Planet Inter 150:213–225
Thomas AM, Nadeau RM, Bürgmann R (2009) Tremor-tide correlations and near-lithostatic pore pressure on the deep San Andreas Fault. Nature 462:1048–1051
Thurber C, Roecker S, Zhang H, Baher S, Ellsworth W (2004) Fine-scale structure of the San Andreas Fault zone and location of the SAFOD target earthquakes. Geophys Res Lett 31:L12S02
Tietze K, Ritter O, Becken M (2010) Magnetotelluric 3D inversion models from the San Andreas Fault near Parkfield, California. AGU Fall Meeting Abstracts, December 2010, p A2086+
Titus SJ, DeMets C, Tikoff B (2005) New slip rate estimates for the creeping segment of the San Andreas Fault, California. Geology 33:205–208
Toke NA, Arrowsmith JR, Rymer MJ, Landgraf A, Haddad DE, Busch MM, Coyan JA, Hannah A (2011) Late Holocene slip rate of the San Andreas Fault and its accommodation by creep and moderate-magnitude earthquakes at Parkfield, California. Geology 39:243–246
Townend J, Zoback MD (2000) How faulting keeps the crust strong. Geology 28:399–402
Townend J, Zoback MD (2004) Regional tectonic stress near the San Andreas Fault in central and southern California. Geophys Res Lett 31:L15S11
Tréhu AM (1991) Tracing the subducted oceanic crust beneath the central California continental margin: results from ocean bottom seismometers deployed during the 1986 PG&E/EDGE experiment. J Geophys Res 96:6493–6506
Türkoglu E, Unsworth M, Caglar I, Tuncer V, Avsar Ü (2008) Lithospheric structure of the Arabia-Eurasia collision zone in eastern Anatolia: magnetotelluric evidence for widespread weakening by fluids? Geology 36:619–622
Umeda K, McCrank GF, Ninomiya A (2007) Helium isotopes as geochemical indicators of a serpentinized fore-arc mantle wedge. J Geophys Res 112:B10206
Unsworth MJ (2010) Magnetotelluric studies of active continent–continent collisions. Surv Geophys 31:137–161
Unsworth MJ, Bedrosian P (2004a) Electrical resistivity structure at the SAFOD site from magnetotelluiric exploration. Geophys Res Lett 31:L12S05
Unsworth MJ, Bedrosian P (2004b) On the geoelectric structure of major strike-slip faults and shear zones. Earth Planets Space 56:1177–1184
Unsworth MJ, Malin PE, Egbert GD, Booker JR (1997) Internal structure of the San Andreas Fault at Parkfield, California. Geology 25:359–362
Unsworth MJ, Egbert GD, Booker JR (1999) High resolution electromagnetic imaging of the San Andreas Fault in central California. J Geophys Res 104:1131–1150
Unsworth MJ, Bedrosian P, Eisel M, Egbert GD, Siripunvaraporn W (2000) Along strike variations in the electrical structure of the San Andreas Fault at Parkfield, California. Geophys Res Lett 27:3021–3024
Usui Y, Uyeshima M, Ogawa T, Yoshimura R, Oshiman N, Yamaguchi S, Toh H, Murakami H, Uto T, Kanezaki H, Mochido Y, Aizawa K, Tanbo T, Mogami T, Ogawa Y, Nishitani T, Sakanaka S, Mishina M, Satoh H, Goto T, Kasaya T, Mogi T, Yamaya Y, Harada M, Shiozaki I, Honkura Y, Koyama S,

Mochiduki H, Nakao S, Wada Y, Fujita Y (2010) Deep resistivity structure beneath the Atotsugawsa fault area in the Niigata Kobe Tectonic zone revealed by a joint Inversion combining wideband- and network-MT surveys. In: 20th international workshop on electromagnetic induction, Giza, Egypt

Wannamaker PE, Grant Caldwell T, Jiracek George R, Maris Virginie, Hill Graham J, Ogawa Yasuo, Bibby Hugh M, Bennie Stewart L, Heise Wiebke (2010) Fluid and deformation regime of an advancing subduction system at Marlborough, New Zealand. Nature 460:733–736

Weckmann U, Ritter O, Haak V (2003) A magnetotelluric study of the Damara Belt in Namibia: 2 MT phases over 90° reveal the internal structure of the Waterberg Fault/Omaruru Lineament. Phys Earth Planet Inter 138:91–112

Wheelock B, Constable S, Key K (2010) A marine electromagnetic study of the continental margin in central California, USA. In: 20th international workshop on electromagnetic induction, Giza, Egypt

Wiersberg T, Erzinger J (2007) A helium isotope cross-section study through the San Andreas Fault at seismogenic depths. Geochem Geophys Geosyst 8:Q01002

Wiese H (1962) Geomagnetische Tiefentellurik Teil ii: Die Streichrichtung der Untergrundstrukturen des elektrischen Widerstandes, erschlossen aus geomagnetischen Variationen. Geofis. Pura e Appl 52:83–103

Wilson DS, McCrory Patricia A, Stanley Richard G (2005) Implications of volcanism in coastal California for the Neogene deformation history of western North America. Tectonics 24:TC3008

Yoshimura R, Oshiman N, Uyeshima M, Toh H, Uto T, Kanezaki H, Mochido Y, Aizawa K, Ogawa Y, Nishitani T, Sakanaka S, Mishina M, Satoh H, Goto T, Kasaya T, Yamaguchi S, Murakami H, Mogi T, Yamaya Y, Harada M, Shiozaki I, Honkura Y, Koyama S, Nakao S, Wada Y, Fujita Y (2009) Magnetotelluric transect across the niigata-kobe tectonic zone, central Japan: a clear correlation between strain accumulation and resistivity structure. Geophys Res Lett 36:L20311

Yoshino T, Noritake F (2011) Unstable graphite films on grain boundaries in crustal rocks. Earth Planet Sci Lett 306(3–4):186–192

Zhang H, Thurber C, Bedrosian P (2009) Joint inversion for vp, vs, and vp/vs at SAFOD, Parkfield, California. Geochem Geophys Geosyst 10:Q11002

Zoback M, Townend J, Grollimund B (2002) Steady-state failure equilibrium and deformation of intraplate lithosphere. Int Geol Rev 44:383–401

Zoback M, Hickman S, Ellsworth W (2006) Structure and properties of the San Andreas Fault in central California: preliminary results from the SAFOD experiment. In: Geophysical Research Abstracts, vol 8. EGU

Zoback M, Hickman S, Ellsworth W (2010) Scientific drilling into the San Andreas Fault zone. Eos Trans AGU 91:197–199